Manuscript Title: Evidence for genetically distinct direct and indirect spinocerebellar pathways mediating proprioception.

Abbreviated Title: Direct and indirect spinocerebellar pathways.

Author names and affiliations:

Iliodora V. Pop[1], Felipe Espinosa[1], Megan Goyal[1], Bishakha Mona[1], Mark A. Landy[1], Osita W. Ogujiofor[1], Kevin M. Dean[2], Channabasavaiah B. Gurumurthy[3, 4], Helen C. Lai[1]

[1] Dept. of Neuroscience, UT Southwestern Medical Center, Dallas, TX 75390

[2] Dept. of Cell Biology, UT Southwestern Medical Center, Dallas, TX 75390

[3] Mouse Genome Engineering Core Facility, University of Nebraska Medical Center, Omaha, NE 68198

[4] Department of Pharmacology and Experimental Neuroscience, College of Medicine, University of Nebraska Medical Center, Omaha, NE 68198

Corresponding author: Helen C. Lai, Helen.Lai@utsouthwestern.edu.

Number of Pages: 42 Number of words for Abstract: 246

Number of Figures: 8 Number of words for Introduction: 1155

Number of Tables: 0 Number of words for Discussion: 2366

Number of Multimedia: 6 Number of 3D Models: 0

Acknowledgments: This work was supported by R01MH120131 and R34NS121873 to K.M.D., R35HG010719 and R21GM129559 to C.B.G., and R01NS100741 to H.C.L. We thank Lin Gan for the *Atoh1*$^{Cre/+}$ knock-in mouse, Martyn Goulding for the *Cdx2::FLPo* mouse, Mark Behlke and Sarah Jacobi from Integrated DNA Technologies for providing pre-production megamers, Rebecca Seal for the *Vglut1* ISH probe, Qiufu Ma for the *Vglut2* ISH probe, Thomas Jessell for the *Gdnf* ISH probe, Heankel Cantu Oliveros and Wei Xu for the Lenti^{FugE}-Cre virus, Christine Ochoa for technical assistance, Neuroscience Microscopy Facility which is supported by the UTSW Neuroscience Dept. and the UTSW Peter O'Donnell, Jr. Brain Institute, LifeCanvas Technologies for tissue clearing assistance, and Jane Johnson, Peter Tsai, Ariel Levine, Euiseok Kim, and the Lai Lab for helpful discussions and careful reading of the manuscript.

Conflict of Interest: The authors declare no competing financial interests.

Abstract

Proprioception, the sense of limb and body position, generates a map of the body that is essential for proper motor control, yet we know little about precisely how neurons in proprioceptive pathways develop and are wired. Proprioceptive and cutaneous information from the periphery is sent to secondary neurons in the spinal cord that integrate and relay this information to the cerebellum either directly or indirectly through the medulla. Defining the anatomy of these direct and indirect pathways is fundamental to understanding how proprioceptive circuits function. Here, we use genetic tools in mice to define the developmental origins and unique anatomical trajectories of these pathways. Developmentally, we find that Clarke's column (CC) neurons, a major contributor to the direct spinocerebellar pathway, derive from the *Neurog1* progenitor domain. By contrast, we find that two of the indirect pathways, the spino-lateral reticular nucleus (spino-LRt) and spino-olivary pathways, are derived from the *Atoh1* progenitor domain, despite previous evidence that *Atoh1*-lineage neurons form the direct pathway. Anatomically, we also find that the mossy fiber terminals of CC neurons diversify extensively with some axons terminating bilaterally in the cerebellar cortex. Intriguingly, we find that CC axons do not send axon collaterals to the medulla or cerebellar nuclei like other mossy fiber sources. Altogether, we conclude that the direct and indirect spinocerebellar pathways derive from distinct progenitor domains in the developing spinal cord and that the proprioceptive information from CC neurons is processed only at the level of granule cells in the cerebellum.

Significance Statement

We find that a majority of direct spinocerebellar neurons in mice originate from Clarke's column (CC), which derives from the *Neurog1*-lineage, while few originate from *Atoh1*-lineage neurons as previously thought. Instead, we find that spinal cord *Atoh1*-lineage neurons form mainly the indirect spino-lateral reticular nucleus and spino-olivary tracts. Moreover, we observe that mossy fiber axon terminals of CC neurons diversify proprioceptive information across granule cells in multiple lobules on both ipsilateral and contralateral sides without sending axon collaterals to the medulla or cerebellar

nuclei. Altogether, we define the development and the anatomical projections of direct and indirect pathways to the cerebellum from the spinal cord.

Introduction

Proprioception, the sense of limb and body position, is critical to generating an online body state map (Sherrington, 1906; Tuthill and Azim, 2018). Knowing the current positional state of the system allows us to plan future trajectories and assess the outcomes of those motor actions. When proprioception is lost, gross trajectories are maintained, but coordinated limb movement is impaired (Gordon et al., 1995; Abelew et al., 2000; Windhorst, 2007; Akay et al., 2014). Muscle and tendon information detected by proprioceptive sensory neurons, and touch information detected by cutaneous afferents in the periphery, are integrated by secondary neurons in the spinal cord and relayed to the cerebellum through both direct and indirect spinocerebellar pathways (Oscarsson, 1965; Bosco and Poppele, 2001; Jiang et al., 2015). How these direct and indirect pathways either converge or diverge in the cerebellum and what kind of differential information is processed through these pathways is unclear. As an initial step toward understanding proprioceptive circuit function, we first need to define the precise anatomy of the spinocerebellar system. In this study, we use genetic tools in mice to elucidate the development of the direct and indirect spinocerebellar pathways and meticulously detail anatomical aspects of the spinocerebellar system.

Developmentally, two progenitor domains are reported to differentiate into neurons of the direct spinocerebellar pathway: the basic helix-loop-helix (bHLH) transcription factor-expressing progenitor domains *Atoh1* (atonal homolog 1) and *Neurog1* (neurogenin 1)(Bermingham et al., 2001; Gowan et al., 2001; Sakai et al., 2012). These progenitor domains differentiate into two neuronal populations called dorsal interneuron 1 and 2 (dI1 and dI2), respectively. However, the dI1 and dI2 populations are both mixed populations with contralaterally and ipsilaterally-projecting neurons, some of which terminate in the developing pons or medulla as well as the cerebellum (Avraham et al., 2009; Sakai et al., 2012). Furthermore, although *Atoh1*-lineage neurons were reported to project to the cerebellum, we previously found that *Atoh1*-lineage neurons did not form Clarke's column (CC), a major source of neurons for the

direct spinocerebellar pathway (Yuengert et al., 2015). Instead, the soma of *Atoh1*-lineage neurons reside ventrally and laterally to CC neurons. Therefore, we hypothesized that *Atoh1*-lineage neurons might form other direct spinocerebellar neurons such as the lamina V-SCTs or dorsal horn-SCTs (Matsushita and Hosoya, 1979; Edgley and Gallimore, 1988; Bermingham et al., 2001; Yuengert et al., 2015). Our previous work also suggested that CC neurons do not develop from *Atoh1*-lineage neurons, but must originate from an alternate progenitor domain, possibly the *Neurog1*-expressing domain. Therefore, altogether, the precise contribution of *Atoh1*- and *Neurog1*-lineage neurons to the direct or indirect spinocerebellar pathways is unclear.

In addition, anatomically, while gross features of the direct spinocerebellar pathways are known, the structural features of axon collateral projections from this pathway are vague. The direct spinocerebellar pathway is known to consist of the ipsilaterally-projecting dorsal and contralaterally-projecting ventral spinocerebellar tracts (DSCT and VSCT), deriving from several anatomically and molecularly distinct groups of soma in diverse laminae throughout the spinal cord (Matsushita and Hosoya, 1979; Matsushita et al., 1979; Sengul et al., 2015; Baek et al., 2019) where they are thought to convey ongoing locomotor activity (Jiang et al., 2015). A major contributor to the DSCT comes from CC neurons, whose soma reside in the medial aspect of the thoracic to upper lumbar spinal cord (Oscarsson, 1965; Baek et al., 2019). While SCT axons terminate as mossy fiber (MF) terminals on granule cells (GCs) in the vermis of the anterior zone (AZ, lobules I-V), the posterior zone (PZ, lobules VIII and anterior IX), and the copula pyramidis (Cop) (Arsenio Nunes and Sotelo, 1985; Bosco and Poppele, 2001; Reeber et al., 2011), it is unclear whether SCT neurons send axon collaterals to areas of the medulla or cerebellar nuclei (CN)(Medial, Interpositus, and Lateral) as is seen from other MF sources, thus allowing for integration with other ascending or descending pathways (Sillitoe et al., 2012; Beitzel et al., 2017). Axon collaterals to the lateral reticular nucleus (LRt) from the direct spinocerebellar pathway have been found in teleosts; however, it is unclear whether this occurs in mammals (Ekerot and Oscarsson, 1976; Szabo et al., 1990; Jiang et al., 2015). Furthermore, studies conflict on whether

SCTs make collateral connections to CN (Matsushita and Ikeda, 1970; Matsushita and Gao, 1997; Mogensen et al., 2017; Luo et al., 2018).

Compared to the direct spinocerebellar pathways, less is known about the development and anatomy of the indirect spino-LRt and spino-olivary pathways. Multiple progenitor domains have been found thus far to contribute to the spino-LRt pathway and anatomically, spino-LRt neurons project ipsilaterally and contralaterally to the LRt in the medulla where they are involved in posture, reaching, and grasping (Alstermark and Ekerot, 2013; Azim et al., 2014; Pivetta et al., 2014; Jiang et al., 2015). The LRt neurons then project either ipsilaterally or contralaterally to terminate in the cerebellar cortex as MFs. To the best of our knowledge, the progenitor domains developing into the spino-olivary tract (Helweg's tract) are unknown; however, anatomically, spino-olivary neurons reside in lamina V-VII of the spinal cord and project contralaterally to the inferior olive (IO) in the medulla (Oscarsson and Sjolund, 1977b, a; Berkley and Worden, 1978; Swenson and Castro, 1983b, a). The neurons in the IO then project contralaterally as well to synapse as climbing fiber (CF) axons onto Purkinje cells (PCs) in the cerebellar cortex (Sillitoe et al., 2012). Thus, ultimately, information from one side of the body ends up ipsilaterally in the cerebellum through the spino-olivary-cerebellar pathway because of the two sets of crossing neurons. While the function of spino-olivary neurons has not been directly tested, neurons in the IO are thought to be involved in the timing of motor commands, motor learning, and error correction (Sillitoe et al., 2012; White and Sillitoe, 2017).

The anatomical architecture of the spinocerebellar system serves as an important foundation for understanding how proprioceptive circuits function. However, as noted above, many details of the development and anatomy of the direct and indirect spinocerebellar pathways remain unanswered. In our study, we seek to provide clarity to these questions by following the lineages of the *Atoh1*- and *Neurog1*-expressing progenitor domains and using a variety of genetic, whole tissue clearing and imaging, and tracing tools to address details of the anatomy. We find that CC neurons develop from the *Neurog1* progenitor population and although CC axons do not collateralize to any structures within the medulla or to the CN, they do collateralize extensively within the cerebellar cortex with some even

crossing the midline within the cerebellum. Furthermore, we find that a majority of spinal cord *Atoh1*-lineage neurons project to the LRt and IO making the indirect spino-LRt and spino-olivary tracts rather than the direct lamina V-SCTs or dorsal horn SCTs as originally hypothesized (Matsushita and Hosoya, 1979; Matsushita et al., 1979; Edgley and Gallimore, 1988; Edgley and Jankowska, 1988; Yuengert et al., 2015). Altogether, in this study, we define novel insights into the development and anatomy of direct and indirect spinocerebellar pathways.

Materials & Methods

Mouse strains

The following mouse strains were used: *Gdnf*$^{fIRES2\text{-}CreERT2}$ (Cebrian et al., 2014)(JAX #024948), *Neurog1BAC-Cre* (Quinones et al., 2010)(JAX #012859), *Atoh1*$^{P2A\text{-}FLPo/+}$ (described here), *Atoh1*$^{Cre/+}$ knock-in (Yang et al., 2010), *R26*$^{LSL\text{-}LacZ/+}$ (Soriano, 1999)(JAX #003474), *R26*$^{LSL\text{-}EYFP/+}$ (Ai3)(JAX #007903)(Madisen et al., 2010), *R26*$^{LSL\text{-}tdTom/+}$ (Ai14)(JAX #007914)(Madisen et al., 2010), *R26*$^{LSL\text{-}FSF\text{-}tdTom/+}$ (Ai65)(JAX #032864)(Madisen et al., 2015), *Cdx2::FLPo* (Bourane et al., 2015). All mice were outbred and thus, are mixed strains (at least C57Bl/6J, C57Bl/6N, and ICR). *Atoh1*$^{Cre/+}$ knock-in mice crossed to *Cdx2::FLPo* and dual recombinase tdTomato reporter Ai65 mice were screened for "dysregulated" expression as previously reported (Yuengert et al., 2015). Tamoxifen (Sigma) was injected at P7 for the *Gdnf*$^{fIRES2\text{-}CreERT2}$ line unless otherwise noted (10 mg/mL dissolved in sunflower oil (Sigma) with 10% ethanol). All animal experiments were approved by the Institutional Animal Care and Use Committee at UT Southwestern.

The *Atoh1*$^{P2A\text{-}FLPo/+}$ mouse was generated using the Easi-CRISPR approach (Quadros et al., 2017). Briefly, a long single stranded DNA cassette consisting of a viral peptide self-cleaving sequence (P2A, porcine teschovirus-1 2A) (Kim et al., 2011) and the codon optimized flippase recombinase sequence (FLPo) were inserted after the last amino acid codon and before the stop codon of *Atoh1*. C57Bl/6N zygotes were microinjected with ribonucleoprotein complexes of Cas9 protein, tracrRNA, and crRNA (5' TGA CTC TGA TGA GGC CAG TT 3') along with a ssDNA megamer for homologous recombination (1497 b.p. containing 60 b.p. each 5' and 3' homology arms and the P2A-FLPo

sequence)(reagents were procured from IDT, microinjection service was provided by the UTSW Transgenic Mouse Core Facility). Assembling CRISPR reagents and microinjections were performed as previously described (Jacobi et al., 2017; Miura et al., 2018). The live born mice were first screened for insertion of the P2A-FLPo sequence and of those that were positive, one of the mice contained the full length cassette. The cassette contained a minor mutation at the end of FLPo (the last isoleucine amino acid was changed to a serine), which could have occurred possibly due to an imprecise DNA repair event. Nevertheless, this amino acid change does not seem to affect the enzymatic function of FLPo. For genotyping, wildtype 321 b.p. and mutant 642 b.p. PCR products were detected using the following primers: WT For 5' CCC TAA CAG CGA TGA TGG CAC AGA AGG 3', WT Rev 5' GGG GAT TGG AAG AGC TGC AGC CGT C 3', and MUT Rev 5' CGA ACT GCA GCT GCA GGC TGG ACA CG 3'. Note that because the P2A sequence self-cleaves near its C-terminus, 21 amino acids of the P2A sequence is fused to the C-terminus of ATOH1.

Tissue processing

Mice are age P0 on the day of birth. Mice older than P10 were anesthetized with Avertin (2,2,2-Tribromoethanol) (0.025-0.030 mL of 0.04 M Avertin in 2-methyl-2-butanol and distilled water/g mouse) and transcardially perfused, first with 0.012% w/v Heparin/PBS and then 4% PFA/PBS. A dorsal or ventral laminectomy exposed the spinal cord to the fixative. Spinal cords were fixed for 2 hrs and the brains overnight at 4°C. Tissue was washed in PBS for at least one day and cryoprotected in 30% sucrose dissolved in deionized water. Tissue was marked with 1% Alcian Blue in 3% acetic acid on one side to keep orientation and were embedded in OCT (Tissue-Tek Optimal Cutting Temperature compound). Tissue was sectioned using a Leica CM1950 Cryostat.

Immunohistochemistry (IHC) and confocal imaging

Cryosections (30-40 μm) were blocked with PBS/1-3% normal goat or donkey serum (Jackson labs)/0.3% Triton X-100 (Sigma) for up to 1 hr at room temperature (RT) and incubated overnight with primary antibody at 4°C. After washing 3 times with PBS, the appropriate secondary antibody (Alexa 488, 567, and/or 647, Invitrogen) was incubated for an hour at RT. Sections were rinsed 3 times in

PBS, mounted with Aqua-Poly/Mount (Polysciences Inc.), and coverslipped (Fisher). The following primary antibodies and dilutions were used: 1:500 rabbit anti-dsRed (Clontech), 1:500 mouse anti-NEUN (Millipore Sigma), 1:500 chicken anti-GFP (Aves), 1:1000 guinea pig anti-VGLUT1 (Millipore Sigma), 1:1000 guinea pig anti-VGLUT2 (Millipore Sigma), 1:100 goat anti-CHAT (Millipore Sigma). Sections were referenced to the Mouse Brain Atlas (Paxinos and Franklin, 2007) and Christopher Reeves Spinal Cord Atlas (Watson et al., 2009).

Fluorescent images were taken on a Zeiss LSM710 or LSM880 confocal microscope with an optical slice of 0.5-10 μm depending on the objective used (10x air, 20x air, 40x oil, or 63x oil). Images were pseudocolored using a magenta/yellow/blue, magenta/green/blue, or magenta/yellow/cyan color scheme using Adobe Photoshop (Adobe) or Fiji (Schindelin et al., 2012). For the mapping of CC thoracolumbar MF terminals (Fig. 4D-G, I-J), confocal images of 30 μm cryosections were analyzed in Fiji using the ROI Manager to label individual MF terminals and the SlideSet PlugIn to export the ROIs as a .svg file (Schindelin et al., 2012; Nanes, 2015). These mapped MF terminals were then overlaid on a traced drawing of the confocal image in Adobe Illustrator.

In situ hybridization (ISH)

ISH was performed as per standard protocols. Detailed protocol is available upon request. Briefly, spinal cord sections (30 μm) were dried at 50˚C for 15 min. then fixed in 4% paraformaldehyde (PFA) in DEPC-PBS for 20 min. at RT. The sections were washed in DEPC-PBS for 5 min. at RT before and after the incubation in RIPA buffer (150 mM NaCl, 1% NP-40, 0.5% Na deoxycholate, 0.1% SDS, 1 mM EDTA, 50 mM Tris pH 8.0) for 60 min. Next, the sections were postfixed in 4% PFA in DEPC-PBS for 15 min at RT. The sections were then washed in DEPC-water followed by acetylation (500 μL of acetic anhydride in 200 mL of 0.1 M RNase-free triethanolamine-HCl at pH 8.0), washed in DEPC-PBS for 5 min., and prehybridized for 2 h at 60-62°C. Sections were incubated overnight at 60-62˚C with 1–2 ng/μL of fresh probe (*Gdnf*, *Vglut1*, or *Vglut2*). A series of low and high stringency washes in 2x and 0.2X SSC as well as treatment with RNaseA and RNase T1 were performed. The sections were blocked in 10% inactivated sheep serum for 1 h followed by overnight incubation with

1:1000 anti-digoxygenin (DIG) antibody (Roche). The sections were washed in PBT and incubated with NBT/BCIP (Roche) staining solution. After the blue precipitate formed, the slides were washed in PBS and coverslipped with Aqua-Poly/Mount (Polysciences Inc.) mounting media. If ISH was followed by IHC, the sections were placed in PBS and then immunostained with 1:500 anti-GFP antibody (Aves) following the IHC protocol described above.

The RNAscope Fluorescent Multiplex Assay (Advanced Cell Diagnostics Inc., Hayward, CA) was performed according to the manufacturer's instructions using a *Vglut1* probe (ACDBio, 416631). All incubation steps were performed in a HybEZ™ II oven set to 40°C. The sections were pretreated by boiling in 1X Target Retrieval solution for 5 minutes. The slides were then washed with distilled water three times and incubated with Protease III for 40 sec. Slides were then washed with distilled water three times and incubated with the probe targeting *Vglut1* for 2 hours. The slides were washed two times thoroughly using 1X wash buffer for 2 min, then incubated with Amp 1-Fl for 30 minutes. The same process (washing then treatment) was repeated for Amp 2-Fl, Amp 3-Fl and Amp 4-Fl for 15, 30 and 15 minutes, respectively. For antibody staining of β-galactosidase, the sections were transferred to a humidified tray and blocked for 30-45 minutes in 0.25mL/slide of PBT (PBS with 0.3% Triton) containing 1% goat serum (Jackson ImmunoResearch). The sections were incubated with chicken anti-β-Galactosidase antibody (Abcam, 1:500) in PBT with 1% goat serum overnight at 4°C. The slides were then washed three times in PBS for 10 minutes and incubated at room temperature for 1 hour with goat anti-chicken Alexa Fluor 488 (Life Technologies, 1:500). Slides were washed three times in PBS for 10 minutes and coverslipped using 2 drops of Aqua-Poly/Mount (Polysciences, Inc.) as the mounting media.

X-gal staining

Slides with spinal cord sections (30 μm) were incubated in staining solution with 5mM $K_3Fe(CN)_6$, 5mM $K_4Fe(CN)_6$ and 1 mg/mL of X-gal (Roche) until precipitate was sufficient to visualize. Sections were moved to PBS, mounted, and coverslipped.

Viral Injections

Mice aged P7-P8 were anesthetized using isoflurane (Henry Schein) and prepared for injections into the spinal cord. The back hair was shaved and 70% ethanol and betadine (Avrio Health L.P.) applied. A midline incision was made on the dorsal surface of the spinal cord. AAV9.hSyn.DIO.eGFP.WPRE.hGH (100 nL total in 27.6 nL increments at 1-2 min intervals (Nanoject II, Drummond Scientific), 1.07 x 10^{13} GC/mL, Penn Vector Core) was injected into the lower thoracic spinal cord through the intervertebral space of P7 or P8 *Gdnf*^{Tom} mice. Lenti^{FugE}-Cre was injected into the lower thoracic to lumbar area of P7 *Atoh1*$^{P2A\text{-}FLPo/+}$*;R26*$^{LSL\text{-}FSF\text{-}tdTom/+}$ mice (total of 50.6 nL in 27.6 nL increments at 1-2 min intervals). Lenti^{FugE}-Cre was pseudotyped with a fusion glycoprotein enabling efficient retrograde axonal transport (Kato et al., 2014). To generate Lenti^{FugE}-Cre, *Cre* was sub-cloned into the third generation HIV-based lentivirus vector under the control of a synapsin promoter (FSW-*Cre*). FSW-*Cre* was co-transfected into HEK293 cells with three packing plasmids, pMDLg/pRRE, pRSV-Rev and pCAGGS-FuG-E to generate Lenti^{FugE}-Cre, which was concentrated with ultracentrifugation to 2.0 x 10^{12} Vg/mL. The incision was closed with surgical glue (Henry Schein). Carprofen (5 mg/kg) was administered daily 3 days after surgery. Spinal cords were harvested approximately 3 weeks after injection.

CTB and FG Injections

Two *GDNF*^{Tom} female mice were injected with 1% (w/v) of either CTB-488 (on the left side) or CTB-647 (on the right side) (Thermo Fisher Scientific). Mice were anesthetized with isoflurane and the area above and around the cerebellar region was prepared for surgery. A midline incision of 0.75 cm and a craniectomy of approximately 1 mm X 1 mm was performed. Bilateral injections at 4 sites were done at (from Bregma): rostrocaudal -5.7 and -6.2 mm and at mediolateral ± 0.35 mm. At each site, several injections in 32 nL increments were performed every 300 μm along the dorsoventral axis at coordinates: -1.8 and -1.5 mm deep for a total of 320 nL of conjugated CTB. Animals were harvested 5 days after injection.

Fluorogold (FG) was injected into the vermis of lobules I-V in the cerebella of *Atoh1*^{Cdx2} or *Atoh1*^{Tom} mice. Mice (1-2 months old) were injected with 4% (w/v) FG solution in saline (Fluorochrome).

Mice were anesthetized with isoflurane and the area above and around the cerebellar region was prepared for surgery. A midline incision of 0.75 cm and a craniectomy of approximately 1 mm wide by 1.5 mm long was performed. For *Atoh1*^{Tom} mice, bilateral injections at six sites were done at (from Bregma): rostrocaudal -5.5, -5.9, and -6.3 mm and at mediolateral ± 0.2-0.4 mm. At each site, several injections in 50.6 nL increments were performed every 300 μm along the dorsoventral axis starting at -1.7 mm deep for a total of 270-720 nL of FG on each side. For *Atoh1*^{Cdx2} mice, bilateral injections at six sites were done at (from Bregma): rostrocaudal -5.6, -5.9, and -6.25 mm and at mediolateral ± 0.4 mm. The maximum depth at each rostrocaudal site was -2.0 mm, -2.4 mm, -1.5 mm, respectively. Multiple injections were done at each site in 32 nL increments along the dorsoventral axis for a total of 384 nL each side. Animals were harvested 7 days after injection.

Whole tissue imaging

Mouse hindbrain and spinal cords were processed following the SHIELD protocol (Park et al., 2018). Tissues were cleared with SmartClear II Pro (LifeCanvas Technologies, Cambridge, MA) for several days, mounted in a gel of 0.9% agarose in EasyIndex (LifeCanvas Technologies), and then incubated in EasyIndex for refractive index matching. Tissues were imaged at 3.6X using a SmartSPIM light sheet microscope (LifeCanvas Technologies). Spinal cords and hindbrain of two female *GDNF*^{Tom} mice (ages P23 and P30) were imaged with 1.8 μm x 1.8 μm x 2 μm sampling (X, Y, and Z, respectively). The total number of 2 μm image slices for each sample is as follows: 1500 slices for CC#1 Spinal Cord (Movie 1), 2700 slices for CC #1 Hindbrain (Movie 2), 1800 slices for CC #2 Spinal Cord (Movie 3), 3900 slices for CC #2 Hindbrain (Movie 4). All hindbrain and spinal cord samples were cut to less than 2.2 cm to fit in the imaging chamber. Movies were made in arivis Vision4D 2.12.6. Maximum intensity projections (MIPs) were processed using Fiji (Schindelin et al., 2012).

Experimental Design and Statistical Tests

The percentage of total CTB^{+} cells and those that are CTB^{+}TOM^{+} were counted from 7-8 regularly spaced sections each from the spinal cords of two female *Gdnf*^{Tom} mice (Fig. 1F). The percentage of total FG^{+} cells and those that are FG^{+}TOM^{+} were counted from 53-72 regularly spaced

sections along the rostral-caudal axis each from the spinal cords of two female *Atoh1*^{Tom} mice and one female *Atoh1*^{Cdx2} mouse (Fig. 1L). Because the *Atoh1*^{Cdx2} mouse does not have any TOM^{+} cells in the upper cervical spinal cord, FG^{+}TOM^{+} counts in the cervical areas (C1-8) were only from the two *Atoh1*^{Tom} mice.

To count the number of MF terminals in *Atoh1*^{Cdx2} with *Gdnf*^{Tom} mice (Fig. 1R), 3 comparable sections from the anterior vermis and 1 comparable section from the posterior vermis were counted to get the number of terminals in anterior zone (AZ, lobules I-V) and posterior zone (PZ, lobules VIII and anterior IX), respectively, from three *Atoh1*^{Cdx2} (1 female, 2 male) mice and two *Gdnf*^{Tom} mice (1 female, 1 male).

The mossy fiber (MF) to cell body ratio (Fig. 3I) was counted from one female (age P23) cleared spinal cord and hindbrain. Cells bodies in the spinal cord and MFs in the cerebellar cortex were counted from 100 μm MIP images of cleared tissue. The ratio calculated is an estimate given that it is impossible to accurately count all the cell bodies and MF terminals and there are many opportunities for over- or undercounting. For example, although cell bodies and mossy fibers were counted only when they could be discretely identified, some MF terminals might appear as two MF terminals, when they in fact come from the same MF. As an example of undercounting, cell bodies and mossy fibers may overlap in the z axis of the 100 μm MIP and may be counted as one instead of several. Altogether, cell bodies and MFs were counted to get an estimate rather than an exact count of the MF/cell body ratio.

Counts of the distribution of infected cells of AAV9-Syn-DIO-EGFP injected in *Gdnf*^{Tom} mice were taken from two male mice (Fig. 4C and H). The number of GFP^{+} cells per length of spinal cord (mm) were counted from 9-16 sections per spinal cord region. Spinal cord regions included T5-6, T7-8, T9, T10-11, T12-13, L1-2, and L3-4.

For experiments injecting Lenti^{FugE}-Cre into *Atoh1*$^{P2A\text{-}FLPo/+}$*;R26*$^{LSL\text{-}FSF\text{-}tdTom/+}$ mice, cell bodies and axons in the left and right lateral funiculi (LF) and ventral funiculi (VF) were counted from 3 female and 1 male mice (Fig. 6D-E). Cell bodies were counted from 13-30 sections per spinal cord region (C6-8, T1-4, T5-7, T8-10, T11-13, L1-3, L4-6, S). Cell bodies per length of spinal cord tissue (mm) were

calculated by counting the number of TOM+ cell bodies and dividing by the length of spinal cord that was covered by that number of sections (i.e. # sections * 30 μm/section = length of spinal cord). Axons were counted from the right and left LF and VF from 1 section/spinal cord region. To estimate the total number of cells infected from C6-S (Fig. 6B), 20% of the spinal cord was counted from each spinal cord region. The estimated total number of cells was then calculated by taking the number of cells counted per number of sections counted times the total number of sections possible for a given spinal cord region and multiplying by 5 (since 20% of the spinal cord was counted).

All data and graphs were processed in Microsoft Excel 2015 and GraphPad Prism 8. Mean ± SEM is reported throughout the manuscript. Note that SEM for n=2 equals the range between the two points.

Results

Clarke's column is the major direct spinocerebellar pathway in mice.

To assess the spinocerebellar system in mice, we identified genetic tools that reproducibly label spinal cord neurons and evaluated their contribution to the spinocerebellar system using a combination of retrograde and anterograde tracing. Previously, we found that the *Atoh1*-expressing progenitor population that makes dI1 neurons, although implicated in making spinocerebellar neurons developmentally (Bermingham et al., 2001; Gowan et al., 2001; Sakai et al., 2012), rarely made CC neurons, which are the major source of the DSCT (Fig. 1A, note the absence of TOM+ cells in the CC area of *Atoh1*-lineage traced neurons, *Atoh1*$^{Cre/+}$*;R26*$^{LSL\text{-}tdTom}$ (Ai14), abbreviated *Atoh1*^{Tom})(Madisen et al., 2010; Yang et al., 2010; Yuengert et al., 2015). Therefore, we sought to identify the progenitor population of CC neurons. Evidence from spinal cord development suggested that the neighboring *Neurog1*-expressing progenitor population that makes dI2 neurons also project to the cerebellum (Avraham et al., 2009; Sakai et al., 2012). Because there are no uniquely specific molecular markers for the dI2 population, we traced the lineage of the entire *Neurog1* population, which includes dI2 neurons and ventral domains, using a transgenic *Neurog1BAC-Cre* strain crossed to a *R26*$^{LSL\text{-}LacZ}$ reporter mouse (Fig. 1A)(Soriano, 1999; Quinones et al., 2010). Large CC cells residing in the medial

thoracic spinal cord colocalize with vesicular glutamate transporter 1 (*Vglut1*) mRNA, a marker for CC (Fig. 1A, B)(Llewellyn-Smith et al., 2007; Malet et al., 2013; Yuengert et al., 2015). In addition, CC is marked by glial derived nerve growth factor (*Gdnf*) as previously reported (Fig. 1B)(Hantman and Jessell, 2010). Because the *Neurog1BAC-Cre* strain labels many neuronal lineages in addition to CC, we decided to use a *Gdnf*$^{IRES2\text{-}CreERT2\ /+}$ mouse line, which has been previously described to specifically label CC neurons, for the remainder of the study (Hantman and Jessell, 2010; Cebrian et al., 2014).

To assess the full complement of direct spinocerebellar projections and how our genetic strains relate to the spinocerebellar system, we retrogradely labeled spinocerebellar neurons with Cholera Toxin subunit B (CTB)-conjugated fluorophores or Fluorogold (FG)(Fig. 1C). These tracers were injected into the cerebella of either CC-labeled (*Gdnf*$^{IRES2\text{-}CreERT2\ /+}$*;R26*$^{LSL\text{-}tdTom}$, abbreviated *Gdnf*^{Tom})(Cebrian et al., 2014) or *Atoh1*-lineage (*Atoh1*^{Tom}) mouse strains targeting the AZ where spinocerebellar neurons are known to project (Arsenio Nunes and Sotelo, 1985; Bosco and Poppele, 2001; Reeber et al., 2011). CTB retrogradely labels CC neurons labeled by *Gdnf*^{Tom} (Fig. 1D-E', arrows). Most CTB-labeled cells reside in CC within thoracic 1-13 (T1-13) of the spinal cord (74 ± 1%, n=2, Fig. 1F). The next most abundant areas of spinocerebellar neurons along the rostral-caudal axis are those in the central cervical (CeCv) nucleus (5 ± 0%)(Cummings and Petras, 1977; Wiksten, 1987; Popova et al., 1995) and cells dorsal of the central canal in T1-13 excluding CC (9 ± 1%), indicating that CC is the most abundantly labeled spinocerebellar projection. Of all CTB-labeled spinocerebellar neurons, 44 ± 12% are labeled with the *Gdnf*^{Tom} line (TOM^{+}). Although the *Gdnf*^{Tom} line labels only a portion of retrogradely CTB-labeled CC neurons (60 ± 16%), almost all the *Gdnf*^{Tom} CC neurons (98 ± 2%) are retrogradely-labeled with CTB. The remaining approximately 40% of CC neurons could be unlabeled by the *Gdnf*^{Tom} line due to incomplete CRE recombination or represent a unique subset of CC neurons.

Next, we wanted to identify whether *Atoh1*-lineage neurons formed direct spinocerebellar projection neurons. In our experience, while CTB is advantageous for restricted labeling in the cerebellum, we noticed that mostly CC neurons were labeled with CTB (Fig. 1F). Therefore, to identify

a broader set of spinocerebellar neurons, we chose to inject FG in *Atoh1*^{Tom} mice, which diffuses more readily and therefore, should cover a wider area of the cerebellum (Fig. 1G). In these mice, we found a similar distribution pattern of FG-labeled cells as our CTB injections (Fig. 1F compared to 1L). Most direct spinocerebellar projections were in CC T1-13 (45 ± 8%, n=3), with other direct spinocerebellar projections mainly from the CeCv (9 ± 2%), dorsal of the central canal in T1-13 (14 ± 2%), and ventral of the central canal in L1-6 (12 ± 4%)(Fig. 1L). In addition, we confirmed that our CTB injections labeled mostly CC neurons compared to FG injections (74 ± 1% vs. 45 ± 8%, respectively). Strikingly, although *Atoh1*-lineage neurons were occasionally labeled with FG (FG$^+$TOM$^+$, Fig. 1K, arrows), only 4 ± 1% of all spinocerebellar (FG$^+$) neurons in the entire spinal cord were *Atoh1*-lineage neurons (FG$^+$TOM$^+$) and only 2 ± 1% of all spinocerebellar neurons were *Atoh1*-lineage neurons within CC. Therefore, we calculate that *Atoh1*^{Tom} neurons make up only 4 ± 1% of FG$^+$ neurons specifically within the CC region.

One possible reason for why so few *Atoh1*^{Tom} neurons were retrogradely-labeled is that *Atoh1*^{Tom} neurons project to areas of the cerebellum not labeled in the FG injections targeting the AZ. To identify the full complement of areas in the cerebellum where *Atoh1*-lineage neurons project, we labeled caudal *Atoh1*-lineage neurons using an intersectional strategy (Fig. 1M, *Atoh1*$^{Cre/+}$; *Cdx2::FLPo*; Ai65, called *Atoh1*^{Cdx2} from hereon). In these mice, *Atoh1*-lineage neurons caudal to approximately cervical 4 (C4) were labeled with tdTomato (Fig. 1O). We scanned coronal sections of the cerebellum every 540 μm and found sparse MF terminals in the GC layers of vermal lobules II-V, VIII, and IX (Fig. 1N and data not shown). Some of these MF terminals were not of CC origin because they were VGLUT1$^-$ (Fig. 1P), while some were VGLUT2$^+$ (Fig. 1Q), consistent with our previous finding that *Atoh1*-lineage neurons are excitatory neurons expressing *Vglut2* mRNA (Yuengert et al., 2015). Compared to CC-labeled neurons (*Gdnf*^{Tom}), *Atoh1*^{Cdx2} neurons had many fewer MF terminals (Fig. 1R, also compare Fig. 1N and Fig. 2A, B). Altogether, our data suggest that CC makes up a majority of spinocerebellar neurons projecting directly to the AZ, while *Atoh1*-lineage neurons make up very few

direct spinocerebellar neurons. Using our genetic tools, we then proceeded to determine the precise anatomy of both CC and *Atoh1*-lineage projections.

Anatomical trajectories of CC neurons.

We used the *Gdnf*^{Tom} line to meticulously trace axonal trajectories of CC neurons to the cerebellum and found several surprising features. First, we found that CC MF terminals in the cerebellum terminate in lobules II-V, VIII, IXa, and Cop (Fig. 2A-C), consistent with the termination locations of spinocerebellar neurons from previous pan-anterograde tracing studies (Arsenio Nunes and Sotelo, 1985; Bosco and Poppele, 2001; Apps and Hawkes, 2009; Reeber et al., 2011). In addition, the three parasagittal stripes in lobule III on both sides of the midline closely matched those found in anterograde tracing studies from the thoracic and lumbar spinal cord (Fig. 2A, B)(Ji and Hawkes, 1994; Reeber et al., 2011). However, while CC axons are known to travel rostrally ipsilaterally in the lateral funiculus of the spinal cord (Oscarsson, 1965 and see Movie 1), we found that several axons appeared to cross the midline within the cerebellum (Fig. 2D, E), suggesting that CC axons terminate both ipsilaterally and contralaterally in the cerebellar cortex, which has been seen occasionally in single-cell reconstructions (Luo et al., 2018). To test whether CC axons from a given CC cell terminates on both sides of the cerebellum, we injected two different CTB fluorophores (CTB-488 and CTB-647) into the left and right sides of the cerebellum (Fig. 1F, G). We found retrogradely labeled cells in CC of the spinal cord that took up both tracers (Fig. 2H, arrows and arrowheads), some of which were colabeled with *Gdnf*^{Tom} (Fig. 2H, arrows). Therefore, CC neurons project ipsilaterally within the spinal cord, but send collaterals to both ipsilateral and contralateral sides in the cerebellar cortex.

Second, we discovered that CC neurons express both *Vglut1*$^{+}$ and *Vglut2*$^{+}$ transcripts using double *in situ* hybridization and immunohistochemistry in *Gdnf*^{EYFP} mice (Fig. 2I, J, arrows). Consistent with the *Gdnf*$^{IRES2\text{-}CreERT2}$ mouse line labeling approximately 60% of all CC cells (Fig. 1F), we find that *Gdnf*^{EYFP} mice label the medial *Vglut1*$^{+}$ neurons in CC while the lateral CC neurons are *Vglut1*$^{+}$ only (Fig. 2I, arrowheads) when the CRE^{ERT2} was activated at P7. Furthermore, we find that CC MF terminals in the cerebellum (TOM^{+}) express both VGLUT1 and VGLUT2 presynaptic markers (Fig. 2K-

L', arrows). Our findings are consistent with a previous report that spinocerebellar neurons are mainly VGLUT2^{+} with some VGLUT1^{+} MF terminals (Gebre et al., 2012).

Lastly, strikingly, we found that CC axons do not make axon collaterals to the cerebellar nuclei, a feature typical of other MF tracts, but has been controversial for the spinocerebellar system (Fig. 3A-F)(Matsushita and Ikeda, 1970; Matsushita and Gao, 1997; Mogensen et al., 2017). In three separate samples, we found no axon terminations in the Medial, Interpositus, or Lateral cerebellar nuclei. Areas near the cerebellar nuclei that had TOM^{+} signal came from axons of passage and are not synaptic terminations (TOM^{+} axons are VGLUT1^{-} or VGLUT2^{-} (Fig. 3A', A'', D', D'')). In summary, our genetic studies of CC neurons show that these glutamatergic neurons terminate bilaterally in the cerebellar vermis, but do not make axon collaterals to the cerebellar nuclei.

Diversification of proprioceptive information through CC neurons.

To obtain a three-dimensional view of CC trajectories, we chemically cleared the spinal cords and hindbrains of two *Gdnf^{Tom}* mice (Supplemental Fig. 3, Movies 1-4). Because *Gdnf* is also expressed in smooth and skeletal muscle (Trupp et al., 1995; Suzuki et al., 1998; Rodrigues et al., 2011), they are prominently labeled with TOM in these samples. In the spinal cords (Movies 1, 3), the CC soma can be seen straddling the midline, while their axons extend to the lateral funiculus (LF) where they make a 90° turn heading rostrally to the cerebellum. Axons in the inferior cerebellar peduncle are also seen traveling directly to the cerebellum (Supplemental Fig. 3F, Movie 4) with no axon collaterals to the pons or medulla.

A feature that was readily apparent from the cleared specimens was the sheer number of MF terminals in the cerebellum indicating an immense diversification of proprioceptive information coming from CC axons (Fig. 3G-H). We counted the number of MF terminals per CC soma in the spinal cord from one cleared sample (spinal cord 1 and hindbrain 1 corresponding to Movies 1 and 2). From these counts, we estimated that there are approximately 81.1 MF terminals in the entire cerebellum for each CC soma (Fig. 3I, orange bar). The MFs terminate largely in vermis I-III (36.3 MF/soma ratio), IV/V (28.2), VIII (5.9), IXa (0.7), and the copula (9.8), consistent with the distribution seen in cryosections

(Fig. 2A-C). The large ratio of MFs to CC soma suggests that CC information is widely distributed within the cerebellum. Furthermore, the proprioceptive information coming into CC neurons require surprisingly few CC neurons to relay that information to the cerebellum. We counted 816 *Gdnf*^{Tom} CC neurons in the spinal cord, which represent around 60% of all CC neurons labeled in the *Gdnf*^{Tom} line, for an estimated 1,360 CC neurons in this mouse spinal cord. This suggests that most of the mouse proprioceptive direct spinocerebellar system comes from roughly a thousand neurons. Unfortunately, the quality of clearing in the other sample (spinal cord 2 and hindbrain 2, Movies 3 and 4) was not adequate for quantification.

Next, we wanted to test whether CC neurons from a restricted area of the spinal cord terminate in discrete or diverse locations in the cerebellum. If a given CC neuron sends MFs terminals to one discrete localized area of the cerebellum, this would suggest that proprioceptive information exists as a traditional homunculus in the cerebellum. However, if a given CC neuron sends MF terminals to multiple areas of the cerebellar cortex, this would provide an anatomical substrate for the fractured somatotopic map that has been detected electrophysiologically (Shambes et al., 1978), where body parts are represented in discontinuous patches across the cerebellum (Manni and Petrosini, 2004; Apps and Hawkes, 2009). To label CC neurons specifically in the thoracolumbar area, we injected AAV9-Syn-DIO-EGFP into *Gdnf*^{Tom} mice (Fig. 4A). Our injections labeled CC neurons on both sides of the spinal cord (Fig. 4B, B', arrows). In two separate injections targeting either the T10-L2 (Fig. 4C) or T12-13 (Fig. 4H) spinal cord, we found that CC neurons from the thoracolumbar spinal cord targeted multiple lobules (II-V, VIII)(GFP^{+} and GFP^{+}TOM^{+}, Fig. 4D-G, I-J, arrows in E'' and J''). Although there were discrete areas that did not contain GFP^{+} cells (arrowheads, Fig. 4D-F), GFP^{+} cells were found over multiple lobules indicating that CC axonal projections from the thoracolumbar spinal cord terminate throughout the cerebellar cortex, consistent with a discontinuous somatotopic map. In addition to terminating across several lobules, we found multiple examples of single axons terminating at regular intervals (50-80 μm) within a GC layer, indicating that a single CC neuron synapses on several GCs

(Fig. 4K-N). Overall, we find that individual CC neurons arborize extensively within the cerebellar cortex, reaching targets over multiple lobules, rather than in discrete locations.

Atoh1-lineage neurons make the spino-LRt and spino-olivary tracts.

Given that *Atoh1*-lineage neurons made few direct spinocerebellar neurons, we sought to identify where in the hindbrain *Atoh1*-lineage axons project. We pursued an intersectional genetic strategy to restrict somatic labeling to caudal *Atoh1*-lineage neurons (*Atoh1*^{Cdx2})(Fig. 5A and Fig. 1O) although we did find sparse ectopic labeling of *Atoh1*-lineage spinal vestibular (SpVe) soma in the hindbrain (Fig. 5C)(Rose et al., 2009). SpVe neurons send descending projections to the spinal cord, therefore, we do not expect that this sparse ectopic labeling interferes with our analysis of ascending projections from caudal spinal cord *Atoh1*-lineage neurons (Liang et al., 2015). In addition, we detect some TOM^{+} axons in the lateral parabrachial nucleus (LPB) in *Atoh1*^{Cdx2} mice (TOM^{+}VGLUT2^{+}, Fig. 5D-D').

Most prominently, we found dense projections of caudal *Atoh1*-lineage neurons in the lateral reticular nucleus (LRt) and inferior olive (IO) (Fig. 5E-H''). To identify whether *Atoh1*^{Cdx2} axons synapse on localized areas of the LRt and IO, we injected FG into the cerebellar AZ (Fig. 5A-B), which retrogradely labels LRt MF and IO CF cell bodies. We found that *Atoh1*^{Cdx2} axons target almost the entirety of the LRt and restricted areas of the IO (IODdf, IOD, IOB, and IOA)(Fig. 5E'-H'). Consistent with our findings, anterograde tracing in rats reports that the spino-olivary tract terminates in the IOD (also called dorsal accessory olive (DAO)) and subnuclei a and b of the caudal medial accessory olive (IOA and IOB, also called cMAO subnuclei a and b) (Swenson and Castro, 1983a; Matsushita et al., 1992; Oldenbeuving et al., 1999). *Atoh1*^{Cdx2} axons colocalize with the presynaptic marker VGLUT2 and are in close apposition to FG labeled neurons in the LRt and IO indicative of synaptic connections (arrows, Fig. 5I-J). Moreover, TOM^{+}VGLUT2^{+} terminals are quite dense in the LRt and IO (Movies 5 and 6) suggesting that many of the synapses might be axo-dendritic rather than axo-somatic. Axon terminations in the LRt and IO was verified in four *Atoh1*^{Cdx2} mice. Altogether, we find that spinal cord

490 *Atoh1*-lineage neurons make mostly the spino-LRt and spino-olivary tracts rather than direct
491 spinocerebellar neurons.
492 *Thoracolumbar Atoh1-lineage neurons project locally.*
493 We next examined whether sparsely labeled thoracolumbar *Atoh1*-lineage neurons send axonal
494 projections to the medulla and cerebellum. Because *Atoh1* is expressed only during development, we
495 pursued an intersectional strategy injecting Lenti$^{FugE\text{-}Cre}$ into *Atoh1*$^{P2A\text{-}FLPo/+}$ mice crossed to an
496 intersectional tdTomato reporter (*R26*$^{LSL\text{-}FSF\text{-}tdTom/+}$). Although we targeted the right spinal cord (orange),
497 we found several cell bodies on the contralateral side were labeled (blue, Fig. 6B), which is likely due to
498 the virus being taken up by axons of passage projecting contralaterally (Fig. 6C). Most of the cell
499 bodies labeled were in the thoracolumbar area (Fig. 6D). Because of the dense ventral projections in
500 our sparsely labeled *Atoh1*-lineage neurons (Fig. 6C, T11-13 and L1-3), we asked whether
501 thoracolumbar *Atoh1*-lineage neurons synapse on motor neurons. We found in all 4 injections a high
502 density of TOM^{+}VGLUT2^{+} puncta (arrowheads, Fig. 6F-F') near and some very closely apposed to
503 CHAT^{+} motor neurons (arrowhead, Fig. 6F'')(representative section shown in Fig. 6F). Some of these
504 TOM^{+}VGLUT2^{+} punta might be axo-dendritic synapses while only a few axo-somatic contacts are
505 detected (Fig. 6F''). Strikingly, we found that axons in the right ventral and lateral funiculi (VF, LF)
506 decreased both rostrally and caudally, suggesting that most of these axons are local projections (Fig.
507 6E) and that few thoracolumbar *Atoh1*-lineage neurons project to the LRt, IO, and cerebellar cortex.
508 Correspondingly, we find only a handful of MF terminals from *Atoh1*-lineage neurons in the GC layer of
509 the cerebellum (representative section shown in Fig. 6G-G', three injections had few MF terminals and
510 one injection had no MF terminals). Thus, we find that thoracolumbar *Atoh1*-lineage neurons primarily
511 project locally, where they synapse onto motor neurons, with few projecting to higher brain regions.
512 **Discussion**
513 In this study, we explore the development and anatomy of direct and indirect spinocerebellar
514 pathways from neurons that derive from *Atoh1* and *Neurog1* progenitor domains and find surprising
515 features of these ascending projections (summarized in Fig. 7). We find that CC neurons, the major

source of neurons for the direct spinocerebellar pathway, are derived from the *Neurog1*-lineage and avoid collateralization to the medulla and CN, while collateralizing extensively in the cerebellar cortex with some axons crossing the midline. Furthermore, we find that axonal projections from thoracolumbar CC neurons project extensively to the AZ and PZ consistent with a fractured somatotopic map. We also discover that *Atoh1*-lineage neurons make up mostly the indirect spino-LRt and spino-olivary pathways while few project directly to the cerebellum. Altogether, we lay the anatomical groundwork to interrogate both the direct and indirect spinocerebellar pathways in future functional studies.

Diversification of proprioceptive information through CC neurons

We find many unique anatomical features of CC neurons that lend insight into how proprioceptive information through CC neurons is relayed. First, we find that relatively few CC neurons (approximately 1,360 total neurons) make up a majority of directly projecting spinocerebellar neurons to the AZ relaying hindlimb proprioceptive information. Although there are several groups of neurons that comprise the direct DSCT and VSCT pathways (Matsushita and Hosoya, 1979; Baek et al., 2019), we find that CC neurons make up 74% (CTB tracer) or 45% (FG tracer) of total retrogradely-labeled neurons from the AZ (Fig. 1F, L). The difference in percentages could be due to the more localized AZ injections with CTB or a preference for CC neurons to take up CTB.

Second, we find that CC neurons synapse only on GCs and do not collateralize to any other areas of the medulla or CN, in contrast to MF terminations that arise from the LRt, red nucleus, and basilar pontine nucleus, which are reported to collateralize to the CN (Sillitoe et al., 2012; Beitzel et al., 2017). Although teleosts have axon collaterals from the direct spinocerebellar pathway to the LRt, we find that CC neurons do not make axon collaterals to the LRt or anywhere else in the pons or medulla, consistent with findings in cats (Ekerot and Oscarsson, 1976; Szabo et al., 1990; Jiang et al., 2015). While MF axons from the spinal cord have been reported to collateralize to the CN, we find that these axon collaterals are not from CC neurons indicating they may be from VSCT or other DSCT neurons (Matsushita and Ikeda, 1970; Matsushita and Gao, 1997). The fact that CC neurons send their information directly to GCs in the cerebellar cortex without collateralization to the LRt or CN suggests

that CC neurons are not involved in integration of inputs involved in posture, reaching or grasping through the LRt or in updating the CN with proprioceptive information.

Third, although CC neurons do not collateralize to the medulla or CN, we do find that within the cerebellar cortex CC neurons extensively diversify their MF terminals between lobules, within a lobule, and even crossing the cerebellum to the contralateral side. Part of the reason for this expansion of proprioceptive information could be for parallel processing across many domains of the cerebellar cortex. Furthermore, our anatomical results are consistent with a fractured somatotopic map proposed from physiological studies that found MF input from a particular region of the body occurred at discontinuous sites within the cerebellum (Shambes et al., 1978). Representative of this extensive diversification, we estimate that there are approximately 81 MF terminals for 1 CC soma (Fig. 3I). In particular, rather than CC neurons from a given area of the spinal cord sending information to discrete areas of the cerebellar cortex in a somatotopic fashion, we found that thoracolumbar CC neurons have axons that spread widely across all CC termination sites (I-V, VIII, IXa, Cop) consistent with findings that the AZ and Cop are connected by axon collaterals (Pijpers et al., 2006; Luo et al., 2018). Altogether, the anatomy of CC neurons suggests a diversification of proprioceptive information to many sites across and within lobules in the cerebellar cortex forming a fractured somatotopic map. We provide evidence that some of this fractured map occurs at the level of spinocerebellar MF inputs to GCs prior to the GC parallel fiber to PC synapse, where further diversification of information is thought to occur (Sillitoe et al., 2012).

Lastly, we find that GCs are likely to be multimodal encoders at the single cell level. The Marr-Albus theory of cerebellar function argues that MF inputs to GCs are mixed such that multimodal inputs to GCs are expanded and recoded allowing for associative memory (Marr, 1969; Albus, 1971). Various anatomical and physiological studies debate whether GCs receive multimodal or unimodal inputs (Ekerot and Jorntell, 2008; Huang et al., 2013). GC neurons have on average 4 dendrites receiving 4 MF inputs and in mice, an individual GC is approximately 40-50 μm from dendrite to dendrite (Gray, 1961; Eccles et al., 1967; Jakab and Hamori, 1988; Huang et al., 2013). We find that at the single cell

level, MF terminals from a given individual CC neuron can form continuous MF rosettes 50-80 μm apart (Fig. 4K-N). These continuous MF rosettes have been reported anecdotally in the literature (Reeber et al., 2011; Houck and Person, 2015; Gilmer and Person, 2017; Luo et al., 2018). The dense MF projections from CC neurons in a single cerebellar stripe argue in favor of a given GC receiving similar inputs as a population; however, our visualization of individual MF axons suggests that an individual GC likely does not receive multiple MF inputs from the same CC neuron supporting the idea that GCs are multimodal encoders at the single cell level.

Atoh1-lineage spino-LRt and spino-olivary neurons

Developmentally, *Atoh1*-lineage neurons were reported to go to the medulla and cerebellum, so we initially hypothesized that *Atoh1*-lineage neurons made lamina V-SCT or dhSCT neurons based on their anatomical location (Matsushita and Hosoya, 1979; Bermingham et al., 2001; Sakai et al., 2012; Yuengert et al., 2015). However, we found instead that *Atoh1*-lineage neurons make mainly indirect spino-LRt and spino-olivary pathways. Thus, the cerebellar axonal projections seen during development either extend to the cerebellum and retract during development or die. Another possibility is that *Atoh1*-lineage neurons do make direct spinocerebellar neurons, but these were undetected for several possible reasons. First, it is possible that *Atoh1*-lineage neurons that make direct spinocerebellar projections derive from cervical 1-4, which are not labeled in our caudal *Atoh1*^{Cdx2} mice. Second, it is possible that the expression of the CRE recombinase in the *Atoh1*$^{Cre/+}$ knock-in mouse is slightly delayed, so we are not capturing the earliest differentiating *Atoh1*-lineage neurons. However, in our previous study, we found fairly good correspondence between *Atoh1* and *Cre* mRNA expression as well as expression of the tdTomato reporter with dI1 neuronal markers (Yuengert et al., 2015). Third, we only retrogradely labeled neurons from the AZ (lobules I-V) and perhaps *Atoh1*-lineage axonal projections to the PZ (Fig. 1R) would be more robustly retrogradely labeled.

For the *Atoh1*-lineage spino-LRt neurons, it will be pertinent to dissect out which spino-LRt neurons they make. Projections to the LRt from the spinal cord are subdivided into 3 major populations: 1) the bVFRT (bilateral ventral reflex tract), contralaterally-projecting neurons whose soma are located

in the cervical and lumbar areas; 2) the PN (propriospinal) neurons, ipsilaterally-projecting neurons that have bifurcating axons to synapse on both motor neurons and the LRt making an internal copy circuit; and 3) the iFT (ipsilateral forelimb tract), ipsilaterally-projecting neurons in the cervical spinal cord (Alstermark and Ekerot, 2013; Azim et al., 2014; Pivetta et al., 2014; Jiang et al., 2015). The PN neurons originate from several genetically-defined progenitor populations and the *Atoh1* progenitor domain can now be added to the list of genetically-defined populations that make the spino-LRt pathway (Azim et al., 2014; Pivetta et al., 2014); however, the progenitor domains that define the remaining bVFRT and iFT tracts are undefined. Because *Atoh1*-lineage neurons consist of both ipsilateral and contralaterally-projecting populations throughout the rostral-caudal axis (Yuengert et al., 2015), they could potentially be any of these three populations. We did find that thoracolumbar *Atoh1*-lineage neurons synapse on motor neurons in the lumbar spinal cord; however, these neurons did not send significant axonal projections past the cervical spinal cord to the LRt.

For the spino-olivary pathway, we found that *Atoh1*-lineage axons target areas of the IO (IODdf, IOD, IOB, IOA) consistent with previously described target areas from anterograde tracing in rats (Swenson and Castro, 1983a; Matsushita et al., 1992; Oldenbeuving et al., 1999). In addition, retrograde tracing from the IO in rats labels cell bodies in laminae V-VIII, some of which are in the approximate location of *Atoh1*-lineage neurons (mainly the medial laminae V-VI)(Swenson and Castro, 1983b; Flavell et al., 2014). However, the distribution of spino-olivary neurons in the spinal cord suggests that there are additional sources of spino-olivary neurons that are not *Atoh1*-lineage.

Comparison of motor behaviors affecting the spino-LRt and spino-olivary-cerebellar pathways

In our previous study, we analyzed the motor behavior of mice that had *Atoh1* deleted caudal to the caudal medulla (*Atoh1* CKO)(Yuengert et al., 2015). In light of our anatomical analysis here, we must reinterpret the motor behaviors from our former study in terms of eliminating *Atoh1*-lineage neurons that contribute to the spino-LRt and spino-olivary pathways. Based on studies manipulating the activity of either spino-LRt neurons or neurons within the IO itself, we can begin to compare the phenotypes in these studies to the *Atoh1* CKO mice. In general, spino-LRt neurons are involved in

posture, forelimb reaching, and grasping (Santarcangelo et al., 1981; Alstermark and Ekerot, 2013; Jiang et al., 2015). Manipulation of the V2a set of propriospinal neurons found deficits in forelimb reaching behavior, but no defect in forelimb paw placement on a horizontal ladder (Azim et al., 2014). In contrast, although we did not assess forelimb reaching behavior, the *Atoh1* CKO mice had a noticeable hunched posture and were impaired in forelimb placement on the ladder assay suggesting that the *Atoh1*-lineage neurons may mediate different components of motor behavior compared to the V2a neurons. For spino-olivary neurons, we are not aware of any studies that have manipulated the activity of these neurons. However, mice that had glutamatergic signaling in IO neurons knocked out had dystonia-like features, such as twisting, stiff limbs, and tremor, and were unable to perform on the accelerating rotarod test (White and Sillitoe, 2017). Although, we did not specifically assay dystonia-like behaviors, we saw no overt twisting, stiff limbs, or tremor in *Atoh1* CKO mice. However, *Atoh1* CKO mice were also completely unable to perform the rotarod test. Notably, the IO glutamatergic KO mice had decreased distance traveled in an open field, while the *Atoh1* CKO mice had more distance travelled. Altogether, the *Atoh1* CKO mice only have a subset of the defects found in other mouse models that manipulate the spino-LRt or IO itself. Therefore, *Atoh1*-lineage neurons must contribute to motor movement in discrete ways. Future experiments dissecting out the function of spino-LRt and spino-olivary components of *Atoh1*-lineage neurons will be an intense area of interest.

Future directions

Accurately defining the connectivity of direct and indirect spinocerebellar projections is fundamental to understanding how proprioceptive and possibly cutaneous information from the hindlimb is processed within the cerebellum. Our study lays the groundwork for several interesting future directions.

Our work and others suggests that the spinocerebellar and spino-LRt systems come from several developmental progenitor domains (Sakai et al., 2012; Azim et al., 2014; Pivetta et al., 2014) and that any given developmental progenitor domain (*Atoh1*, for example) contributes to several neuronal types (minimally, spino-LRt and spino-olivary tracts). Comparing and contrasting features of

neurons with similar anatomical connectivity, but generated from different progenitor domains may lend insights into the varied functions mediated by seemingly similar anatomical classes. Conversely, separating out different pathways, such as the spino-LRt and spino-olivary tracts that are generated from a single progenitor domain (*Atoh1*) will be important for determining the separate functions of these pathways.

Next, we found that direct CC neurons do not send axon collaterals to the LRt or IO and that information to the LRt and IO are coming from *Atoh1*-lineage neurons. Therefore, the MF and CF input coming from the spinal cord into the cerebellar cortex comes from different information streams and are not simply collateral copies of the direct CC pathway. Future work focused on how the direct and indirect information streams from the spinal cord either converge or diverge within the cerebellar cortex will be particularly interesting. Physiological experiments from isolated patches or microzones in the cerebellar cortex have found that MF and CF inputs to GCs and PCs, respectively, are activated by cutaneous receptive fields that correspond to of consistent areas of the body, underlying the one-map hypothesis (Ekerot and Larson, 1980; Garwicz et al., 1998; Brown and Bower, 2001; Voogd et al., 2003; Odeh et al., 2005; Pijpers et al., 2006; Pijpers and Ruigrok, 2006; Apps and Hawkes, 2009; Cerminara et al., 2013). For example, the C1 zone of the copula receives ipsilateral hindlimb and tail input from the lateral IOD CFs in rats and we have shown that the copula is a major termination area of MFs coming from CC neurons in the spinal cord suggesting a convergence of direct CC and indirect CF input to the copula (Atkins and Apps, 1997; Cerminara et al., 2013). Similarly, CF inputs from the hindlimb also go to the AZ, which is another major termination zone for CC neurons, indicating convergence of MF and CF inputs in the AZ (Eccles et al., 1968b, a; Jorntell et al., 2000; Voogd and Ruigrok, 2004). Future studies focused on determining whether MF and CF inputs from the spinal cord go to the same exact patches or microzones in the cerebellar cortex will help define whether MF inputs that generate the fractured somatotopic map converges with CF inputs from the same hindlimb region thus generating one-map (Sugihara and Quy, 2007; Apps and Hawkes, 2009). In addition, physiological studies understanding the relative timing of spinal cord MF and CF inputs to GCs and PCs will lend

672 insight into how the proprioceptive body map through MF inputs and perhaps error information through
673 CF inputs are computed.

674 **Legends**

675 **Figure 1. Clarke's column (CC) is the major direct spinocerebellar pathway in mice.** (A) Lineage
676 tracing of *Neurog1*-expressing progenitors (*Neurog1BAC-Cre* crossed to $R26^{LSL\text{-}LacZ}$) in the neural tube
677 identifies large CC neurons in the thoracic spinal cord (box in X-gal stain). β-Gal expressing cells
678 (green) colocalize with the CC marker, *Vglut1* mRNA (magenta, arrows). *Atoh1*-lineage neurons
679 ($Atoh1^{Tom}$) reside lateral and ventral to CC. (B) CC is marked by expression of *Gdnf* and *Vglut1* mRNA.
680 (C) Diagram of cerebellar injections into the anterior zone (AZ, lobules I-V) with either CTB or fluorogold
681 (FG) into either $Gdnf^{Tom}$ or $Atoh1^{Tom}$ mice to retrogradely label direct spinocerebellar projections. (D-E')
682 CTB injection into vermis lobules III-V of the cerebellum retrogradely labels CC (E, E', green) in the
683 spinal cord and colocalizes with the genetic label for CC ($Gdnf^{Tom}$)(E', CTB^+TOM^+, arrows). (F)
684 Quantitation of the percentage of total CTB^+ cells in a given region of the spinal cord (light orange) with
685 the percentage of CTB^+TOM^+ cells superimposed (dark orange). 74 ± 1% (n=2) of all CTB^+ cells in the
686 spinal cord are in CC T1-13. 44 ± 12% of all CTB^+ cells are TOM^+ in CC T1-13. Therefore, 60 ± 16% of
687 CTB^+ neurons in CC are labeled by $Gdnf^{Tom}$. Spinal cords were divided into cervical (C), thoracic (T),
688 and lumbar (L) areas. The central cervical (CeCv) and CC areas were delineated separately with all
689 other cells categorized based on their C, T, L, S location and whether they were dorsal or ventral to the
690 central canal. (G) FG injected into vermis lobules II-V of $Atoh1^{Tom}$ mice. (H-K) Retrograde labeling from
691 the cerebellum with FG (green) labels CC (I, J) in the thoracic spinal cord, CeCv in the cervical spinal
692 cord (H), and a few other neurons in other areas of the spinal cord (K). Only a few neurons are *Atoh1*-
693 lineage (K, FG^+TOM^+, arrows) with an occasional *Atoh1*-lineage neuron labeling a CC cell (I, FG^+TOM^+,
694 arrowhead) as previously reported (Yuengert et al., 2015). (L) Quantitation of the percentage of FG^+
695 cells in a given region of the spinal cord (light blue) with the percentage of FG^+TOM^+ cells
696 superimposed (dark blue). FG retrogradely labels mostly CC neurons in T1-13 (45 ± 8%, n=3) with 2 ±
697 1% of total FG^+ cells being FG^+TOM^+ in CC T1-13. Therefore, only 4% ± 1% of FG^+ cells in CC T1-13

are labeled with *Atoh1*^{Tom}. (M-N) In mice where caudal *Atoh1*-lineage neurons are labeled (*Atoh1*^{Cdx2}), few mossy fiber (MF) terminals are seen in the cerebellum (N). (O) Spinal cord neurons caudal to C2-5 are labeled with tdTomato (TOM$^+$, magenta) in *Atoh1*^{Cdx2} mice. Few cell bodies in the C2-5 spinal cord area are TOM$^+$ compared to C6-8 and T11-13 sections. NEUN antibody staining (blue) delineates the grey matter of the spinal cord. (P-Q) *Atoh1*^{Cdx2} TOM$^+$ MF terminals are VGLUT1$^-$ (P, arrowheads) and VGLUT2$^+$ (Q, arrows). (R) Counts from comparable sections of *Gdnf*^{Tom} and *Atoh1*^{Cdx2} mice indicate that neurons labeled in *Atoh1*^{Cdx2} mice have considerably fewer MF terminals in lobules I-V (*Gdnf*^{Tom} 2110 ± 183 terminals, n=2 vs. *Atoh1*^{Cdx2} 690 ± 265 terminals, n=3), while MF terminals in lobules VIII/IXa are comparable (*Gdnf*^{Tom} 130 ± 37 terminals vs. *Atoh1*^{Cdx2} 137 ± 55 terminals). Abbrev: P, postnatal. Scale bars: 1 mm (D, G), 100 μm (A, B, E, E', H-K, N, O), 10 μm (P,Q).

Figure 2. Glutamatergic CC mossy fibers terminate ipsilaterally and contralaterally in the cerebellar vermis. (A-C) Coronal sections from *Gdnf*^{Tom} mice reveal CC mossy fiber (MF) terminals (TOM$^+$) in lobules II-V, VIII, IXa, and the copula (C, Cop, arrows). Parasagittal stripes (1, 2, 3) in lobule III are apparent. (D-E) Some CC axons (TOM$^+$) cross the midline (D, arrow, cryosection, and E, arrows, cleared sample, 200 μm maximum intensity projection (MIP)). (F) Diagram of dual CTB-488 and CTB-647 injections in *Gdnf*^{Tom} mice. (G) Coronal section showing the injection site of CTB-488 and CTB-647. (H) CC neurons are co-labeled with the fluorescent CTB injected on the ipsilateral side as well as the fluorescent CTB injected on the contralateral side (arrows and arrowheads, CTB-488$^+$CTB-647$^+$). Some cells also colocalize with the *Gdnf*^{Tom} genetic label for CC (arrowheads, TOM$^+$CTB-488$^+$CTB-647$^+$). (I-J) CC cells in the spinal cord (GFP$^+$ antibody) express both *Vglut1* (*Vg1*) and *Vglut2* (*Vg2*) mRNA (arrows, *Gdnf*^{EYFP} mice, GFP antibody to amplify signal). *Gdnf*^{EYFP} mice injected with tamoxifen at P7 reveal that only a subset of CC is labeled (I, *Vg1*$^+$-only cells, arrowheads). (K-L') CC MF terminals (TOM$^+$) overlap with VGLUT1 (K-K') and VGLUT2 (L-L') stripes in lobule III. K and L panels are neighboring 40 μm sections taken from lobule III indicated in (A, arrow). Abbrev: Med, Medial; Int, Interpositus; Lat, Lateral. Scale bars: 1 mm (A, B, C, G), 100 μm (D, E, H, I, J, K, L), 10 μm (K', L').

Figure 3. CC neurons evade the cerebellar nuclei (CN) and arborize extensively in the cerebellar cortex. (A-D) Almost no CC *Gdnf*^{Tom} axons enter or are near the CN (arrowheads, Med, Int, Lat)(A, B, C, and D are successive sections 160 μm apart). Areas of TOM^{+} signal near CN do not colocalize with presynaptic markers VGLUT1 (A', D') or VGLUT2 (A'', D'') indicating these are axons of passage and not presynaptic terminals. (E) CC axons (TOM^{+}) avoid the CN in another *Gdnf*^{Tom} mouse whose cerebellum was cleared (100 μm MIP). (F) CC axons (TOM^{+}) avoid the CN (40 μm cryosection) in another example *Gdnf*^{Tom} mouse. Images are from two female (A-E) and one male (F) mice (n=3). (G-H) Example images of 100 μm MIP from a *Gdnf*^{Tom} cleared cerebellum. CC MF terminals (TOM^{+}) are seen in II-V, VIII, IXa, and Cop. (I) The total number of MF terminals (grey) were counted from each region of the cerebellum in the cleared sample (n=1, see Material and Methods) and divided by the total number of *Gdnf*^{Tom} CC cell bodies (816 cells) in the spinal cord of the cleared sample (black, MF/cell body ratio). Overall the whole cerebellum (Cb) has an estimated 81.1 MF terminals per CC cell body in the spinal cord (orange bar). Most MF terminals from *Gdnf*^{Tom} CC cells terminate in I-III, IV/V, VIII/IXa, and Cop (blue bars). Abbrev: Med, Medial; Int, Interpositus; Lat, Lateral. Scale bars: 1 mm (G, G', H), 100 μm (H inset, A-F), 10 μm (A'-A'', D'-D'').

Supplemental Fig. 3. Annotated still images from cleared spinal cords and hindbrains. (A-B) Screenshots of spinal cord sample #1. CC cell bodies (soma) cluster around the midline mainly in the thoracic region of the spinal cord (TOM^{+}, magenta). Axons are seen extending toward the LF and extending rostrally. Unidentified midline cells and smooth muscle cells lining blood vessels (*) are labeled with the *Gdnf*^{Tom} mouse line. The meninges also fluoresces. (C-E) Screenshots of hindbrain sample #1. CC axons avoid the cerebellar nuclei and terminate in I-V, VIII, IXa, and Cop. (F) Screenshot of hindbrain sample #2. CC axons are seen traveling rostrally from the spinal cord through the icp. Smooth muscle cells lining blood vessels (*) are prominently labeled in this sample. Time stamp from which the screenshot was taken is in the upper right corner. Abbrev: LF, lateral funiculus; icp, inferior cerebellar peduncle.

748 **Figure 4. Thoracolumbar CC MFs send diverse projections to multiple lobules.** (A-B') Spinal cord
749 injections of AAV9-Syn-DIO-EGFP at lower thoracic levels into *Gdnf*^{Tom} mice labels CC neurons on
750 both sides of the spinal cord (B', arrows). (C) GFP$^+$ cells for one experiment are expressed mainly in
751 the T10-L2 region of the spinal cord. (D-G) Schematics of coronal cerebellar sections of the spinal cord
752 injected from C indicating the location of all CC MF terminations (TOM$^+$, red areas). The subset of CC
753 MF terminations that are from the lower thoracic-lumbar region (GFP$^+$, green, and GFP$^+$TOM$^+$, yellow)
754 are spread over multiple lobules (II-V, VIII). Certain CC MF termination regions do not have
755 thoracolumbar CC neuronal projections (red areas, arrowheads with an absence of any GFP$^+$
756 terminations). (E'-E'') Example of CC MF terminations (TOM$^+$, arrows and arrowhead), some of which
757 are from the thoracolumbar spinal cord (GFP$^+$TOM$^+$, arrows). (H) GFP$^+$ cells in a second injection are
758 expressed mainly in the T12-13 region of the spinal cord. (I-J) Sagittal cerebellar views of the AAV9-
759 Syn-DIO-EGFP-injected *Gdnf*^{Tom} mouse from H. Thoracolumbar CC MF terminals (GFP$^+$, green, and
760 GFP$^+$TOM$^+$, yellow) are spread out over lobules II-V. All CC MF terminals are TOM$^+$ (I-J, red dots). (J'-
761 J'') Thoracolumbar CC MF terminations (GFP$^+$TOM$^+$, arrows) are seen in lobule III. (K-N) Examples of
762 individual MF axons and terminals from three mice: a cleared female mouse sample (K, 76 μm
763 maximum intensity projection (MIP)), one female mouse (L, 40 μm cryosection), and one male mouse
764 (M, N, 40 μm cryosection). Axons appear to have branching points (black arrowheads) and regularly
765 spaced MF terminals (white arrowheads)(K-L). MF terminals from an individual axon are spaced 50-80
766 μm apart (M-N). Scale bars: 100 μm (B, B', E', J', K, L); 10 μm (E'', J'', M, N).
767 **Figure 5. Spinal cord *Atoh1*-lineage neurons make spino-LRt and spino-olivary pathways.** (A)
768 Schematic of FG injections into the AZ of *Atoh1*^{Cdx2} mice to retrogradely label LRt and IO neurons in the
769 medulla. (B) FG injected into lobules I-V. (C) Sparse cell bodies in the SpVe are detected in *Atoh1*^{Cdx2}
770 mice. (D-D'') TOM$^+$ terminals seen in the lateral parabrachial (LPB) nucleus (D) are VGLUT2$^+$ (D'',
771 arrows). (E-H'') A high density of *Atoh1*^{Cdx2} axons from the spinal cord are found in the LRt as well as
772 areas of the IO (IODdf, IOD, IOB, IOA). (I-J) *Atoh1*^{Cdx2} axon terminals (TOM$^+$, magenta) expressing the
773 presynaptic VGLUT2 marker (cyan) are closely apposed to retrogradely labeled cells in the LRt (I) and

774 IO (J)(arrows). Axonal terminations in the LRt and IO were verified in n=4 mice. Representative
775 sections shown in E-H''. Abbrev: ECu, external cuneate nucleus; IO, inferior olive; IOA, inferior olive
776 subnucleus A of medial nucleus; IOB, inferior olive subnucleus B of medial nucleus; IOBe, inferior olive
777 beta subnucleus; IOC, inferior olive subnucleus C of medial nucleus; IOD, inferior olive dorsal nucleus;
778 IODdf, dorsal fold of the IOD; IOM, inferior olive medial nucleus; IOPr, inferior olive principal nucleus;
779 IRt, intermediate reticular nucleus; LRt, lateral reticular nucleus; SpVe, spinal vestibular nucleus. Scale
780 bars: 1 mm (B, D), 100 μm (C, D', E-H''), 10 μm (D'', I, J).

781 **Figure 6. Thoracolumbar *Atoh1*-lineage neurons project locally within the spinal cord.** (A)
782 Diagram of rostral to caudal sections of the spinal cord (left (blue) and right (orange) of the LF (darker
783 shade) and VF (lighter shade)). Lenti^{FugE}-Cre was injected into *Atoh1*$^{P2A\text{-}FLPo/+}$;*R26*$^{LSL\text{-}FSF\text{-}tdTom/+}$ mice,
784 such that only *Atoh1*-lineage neurons in the lower thoracolumbar spinal cord are labeled. (B) Lenti^{FugE}-
785 Cre injections targeted the right thoracolumbar spinal cord. The total estimated number of infected cells
786 (TOM^{+}) was consistent for the right side (786 ± 20 cells, orange, n=4 mice), but was variable for the left
787 side (598 ± 223 cells, blue) where the virus appears to be taken up by axons of passage that project to
788 the contralateral side (see C). (C) Representative sections of the spinal cord from a Lenti^{FugE}-Cre-
789 injected *Atoh1*$^{P2A\text{-}FLPo/+}$;*R26*$^{LSL\text{-}FSF\text{-}tdTom/+}$ mouse. Cell bodies on the right side of the spinal cord and
790 axons in the right LF (dark orange arrowhead) are labeled. Axons in the right VF (light orange
791 arrowhead) appear to be axons from cell bodies that are located on the contralateral side of the spinal
792 cord (blue arrows). Some axons in the left LF (blue arrowhead) are also seen. (D) L1-3 is the site of
793 peak infection (number of TOM^{+} cell bodies labeled per length of spinal cord (mm)) and the number of
794 cell bodies labeled tapers off both rostrally and caudally further away from the injection site. (E) Very
795 few axons on the right side (orange (LF) and light orange (VF)) are detected in rostral sections (C6-8)
796 compared to the site of injection L1-3. (F-F'') Some of the sparsely labeled thoracolumbar *Atoh1*-
797 lineage neurons have presynaptic terminals near (arrowheads, TOM^{+}VGLUT2^{+}) or closely apposed (F'',
798 arrowhead, TOM^{+}VGLUT2^{+}) to motor neurons (CHAT^{+})(detected in n=4 samples, representative image
799 shown). (G-G') Very few MF terminals are detected in the cerebellum. Of the MF terminals that are

detected, they are VGLUT2+ (G'). See Materials and Methods for details of quantitation for B, D, E. Abbrev: LF, lateral funiculus; VF, ventral funiculus. Scale bars: 1 mm (G), 100 μm (C, F), 10 μm (F', G', F'').

Figure 7. Direct and indirect pathways to the cerebellum. (A) *Neurog1*-lineage neurons of the developing neural tube generate CC neurons that project directly from the spinal cord to the cerebellum while *Atoh1*-lineage neurons form both direct and indirect pathways to the cerebellum. (B) Schematic of major anatomical findings. CC neurons (orange) project ipsilaterally mainly from the thoracic spinal cord directly to the cerebellum. Some CC axons cross the midline (dotted orange). *Atoh1*-lineage neurons project mainly to the IO and LRt in the medulla (red and purple). Thoracolumbar *Atoh1*-lineage neurons project mostly within the spinal cord (red, horizontal arrows), although some project to more rostral regions within the medulla and cerebellum (dotted red with purple and red arrowheads). (C-D) Illustrations of direct and indirect spinocerebellar pathways. CC neurons project rostrally in the ipsilateral funiculus where they branch extensively, avoiding the cerebellar nuclei (Med, Int, Lat) to terminate in vermis I-V, VIII, IXa, and Cop (C). Some CC axons cross the midline within the cerebellum. *Atoh1*-lineage neurons in the spinal cord project both ipsilaterally and contralaterally to target mainly the LRt and IO in the hindbrain (D). *Atoh1*-lineage neurons in the thoracolumbar area project mostly locally within the spinal cord. A few of the axons from thoracolumbar *Atoh1*-lineage neurons may project to the medulla (dotted red and purple). Some spinal cord *Atoh1*-lineage neurons reach the AZ (lobules I-V) and PZ (lobules VIII/IXa) of the cerebellar cortex (dotted red). Abbrev: IRt, intermediate reticular nucleus; LRt, lateral reticular nucleus; IO, inferior olive; AZ, anterior zone; PZ, posterior zone.

Multimedia, Figure, and Table

Movie 1. Spinal cord sample 1. *Gdnf*^{Tom} cleared spinal cord.

Movie 2. Hindbrain sample 1. *Gdnf*^{Tom} cleared hindbrain.

Movie 3. Spinal cord sample 2. *Gdnf*^{Tom} cleared spinal cord.

Movie 4. Hindbrain sample 2. *Gdnf*^{Tom} cleared hindbrain.

825 **Movie 5**. **Three-dimensional projection of cells in the LRt of *Atoh1*^{Cdx2} mice.** Cropped cell in Fig. 5I

826 is taken from this z-stack of 0.5 μm optical slices with 0.25 μm step. FG (yellow), *Atoh1*^{Cdx2} axons

827 (TOM^{+}, magenta), VGLUT2 (cyan).

828 **Movie 6**. **Three-dimensional projection of cells in the IO of *Atoh1*^{Cdx2} mice.** Cropped cell in Fig. 5J

829 is taken from this z-stack of 0.5 μm optical slices with 0.25 μm step. FG (yellow), *Atoh1*^{Cdx2} axons

830 (TOM^{+}, magenta), VGLUT2 (cyan).

831

832 **References:**

833 Abelew TA, Miller MD, Cope TC, Nichols TR (2000) Local loss of proprioception results in disruption of
834 interjoint coordination during locomotion in the cat. J Neurophysiol 84:2709-2714.
835 Akay T, Tourtellotte WG, Arber S, Jessell TM (2014) Degradation of mouse locomotor pattern in the
836 absence of proprioceptive sensory feedback. Proc Natl Acad Sci U S A 111:16877-16882.
837 Albus JS (1971) Mathematical biosciences. In, p volumes. New York,: Elsevier.
838 Alstermark B, Ekerot CF (2013) The lateral reticular nucleus: a precerebellar centre providing the
839 cerebellum with overview and integration of motor functions at systems level. A new hypothesis.
840 J Physiol 591:5453-5458.
841 Apps R, Hawkes R (2009) Cerebellar cortical organization: a one-map hypothesis. Nat Rev Neurosci
842 10:670-681.
843 Arsenio Nunes ML, Sotelo C (1985) Development of the spinocerebellar system in the postnatal rat. J
844 Comp Neurol 237:291-306.
845 Atkins MJ, Apps R (1997) Somatotopical organisation within the climbing fibre projection to the
846 paramedian lobule and copula pyramidis of the rat cerebellum. J Comp Neurol 389:249-263.
847 Avraham O, Hadas Y, Vald L, Zisman S, Schejter A, Visel A, Klar A (2009) Transcriptional control of
848 axonal guidance and sorting in dorsal interneurons by the Lim-HD proteins Lhx9 and Lhx1.
849 Neural Dev 4:21.
850 Azim E, Jiang J, Alstermark B, Jessell TM (2014) Skilled reaching relies on a V2a propriospinal internal
851 copy circuit. Nature 508:357-363.
852 Baek M, Menon V, Jessell TM, Hantman AW, Dasen JS (2019) Molecular Logic of Spinocerebellar
853 Tract Neuron Diversity and Connectivity. Cell Rep 27:2620-2635 e2624.
854 Beitzel CS, Houck BD, Lewis SM, Person AL (2017) Rubrocerebellar Feedback Loop Isolates the
855 Interposed Nucleus as an Independent Processor of Corollary Discharge Information in Mice. J
856 Neurosci 37:10085-10096.

857 Berkley KJ, Worden IG (1978) [Projections to the inferior olive of the cat. I. Comparisons of input from
858 the dorsal column nuclei, the lateral cervical nucleus, the spino-olivary pathways, the cerebral
859 cortex and the cerebellum]. J Comp Neurol 180:237-251.
860 Bermingham NA, Hassan BA, Wang VY, Fernandez M, Banfi S, Bellen HJ, Fritzsch B, Zoghbi HY
861 (2001) Proprioceptor pathway development is dependent on Math1. Neuron 30:411-422.
862 Bosco G, Poppele RE (2001) Proprioception from a spinocerebellar perspective. Physiol Rev 81:539-
863 568.
864 Bourane S, Grossmann KS, Britz O, Dalet A, Del Barrio MG, Stam FJ, Garcia-Campmany L, Koch S,
865 Goulding M (2015) Identification of a spinal circuit for light touch and fine motor control. Cell
866 160:503-515.
867 Brown IE, Bower JM (2001) Congruence of mossy fiber and climbing fiber tactile projections in the
868 lateral hemispheres of the rat cerebellum. J Comp Neurol 429:59-70.
869 Cebrian C, Asai N, D'Agati V, Costantini F (2014) The number of fetal nephron progenitor cells limits
870 ureteric branching and adult nephron endowment. Cell Rep 7:127-137.
871 Cerminara NL, Aoki H, Loft M, Sugihara I, Apps R (2013) Structural basis of cerebellar microcircuits in
872 the rat. J Neurosci 33:16427-16442.
873 Cummings JF, Petras JM (1977) The origin of spinocerebellar pathways. I. The nucleus cervicalis
874 centralis of the cranial cervical spinal cord. J Comp Neurol 173:655-692.
875 Eccles JC, Ito M, Szentágothai Jn (1967) The cerebellum as a neuronal machine. Berlin, New York
876 etc.: Springer-Verlag.
877 Eccles JC, Provini L, Strata P, Taborikova H (1968a) Topographical investigations on the climbing fiber
878 inputs from forelimb and hindlimb afferents to the cerebellar anterior lobe. Exp Brain Res 6:195-
879 215.
880 Eccles JC, Provini L, Strata P, Taborikova H (1968b) Analysis of electrical potentials evoked in the
881 cerebellar anterior lobe by stimulation of hindlimb and forelimb nerves. Exp Brain Res 6:171-
882 194.

883 Edgley SA, Gallimore CM (1988) The morphology and projections of dorsal horn spinocerebellar tract
884 neurones in the cat. J Physiol 397:99-111.
885 Edgley SA, Jankowska E (1988) Information processed by dorsal horn spinocerebellar tract neurones
886 in the cat. J Physiol 397:81-97.
887 Ekerot CF, Larson B (1980) Termination in overlapping sagittal zones in cerebellar anterior lobe of
888 mossy and climbing fiber paths activated from dorsal funiculus. Exp Brain Res 38:163-172.
889 Ekerot CF, Jorntell H (2008) Synaptic integration in cerebellar granule cells. Cerebellum 7:539-541.
890 Ekerot CJ, Oscarsson L (1976) The lateral reticular nucleus in the cat. V. Does collateral activation from
891 the dorsal spinocerebellar tract occur? Exp Brain Res 25:327-337.
892 Flavell CR, Cerminara NL, Apps R, Lumb BM (2014) Spino-olivary projections in the rat are
893 anatomically separate from postsynaptic dorsal column projections. J Comp Neurol 522:2179-
894 2190.
895 Garwicz M, Jorntell H, Ekerot CF (1998) Cutaneous receptive fields and topography of mossy fibres
896 and climbing fibres projecting to cat cerebellar C3 zone. J Physiol 512 (Pt 1):277-293.
897 Gebre SA, Reeber SL, Sillitoe RV (2012) Parasagittal compartmentation of cerebellar mossy fibers as
898 revealed by the patterned expression of vesicular glutamate transporters VGLUT1 and
899 VGLUT2. Brain Struct Funct 217:165-180.
900 Gilmer JI, Person AL (2017) Morphological Constraints on Cerebellar Granule Cell Combinatorial
901 Diversity. J Neurosci 37:12153-12166.
902 Gordon J, Ghilardi MF, Ghez C (1995) Impairments of reaching movements in patients without
903 proprioception. I. Spatial errors. J Neurophysiol 73:347-360.
904 Gowan K, Helms AW, Hunsaker TL, Collisson T, Ebert PJ, Odom R, Johnson JE (2001) Crossinhibitory
905 activities of Ngn1 and Math1 allow specification of distinct dorsal interneurons. Neuron 31:219-
906 232.
907 Gray EG (1961) The granule cells, mossy synapses and Purkinje spine synapses of the cerebellum:
908 light and electron microscope observations. J Anat 95:345-356.

909 Hantman AW, Jessell TM (2010) Clarke's column neurons as the focus of a corticospinal corollary
910 circuit. Nat Neurosci 13:1233-1239.
911 Houck BD, Person AL (2015) Cerebellar Premotor Output Neurons Collateralize to Innervate the
912 Cerebellar Cortex. J Comp Neurol 523:2254-2271.
913 Huang CC, Sugino K, Shima Y, Guo C, Bai S, Mensh BD, Nelson SB, Hantman AW (2013)
914 Convergence of pontine and proprioceptive streams onto multimodal cerebellar granule cells.
915 eLife 2:e00400.
916 Jacobi AM, Rettig GR, Turk R, Collingwood MA, Zeiner SA, Quadros RM, Harms DW, Bonthuis PJ,
917 Gregg C, Ohtsuka M, Gurumurthy CB, Behlke MA (2017) Simplified CRISPR tools for efficient
918 genome editing and streamlined protocols for their delivery into mammalian cells and mouse
919 zygotes. Methods 121-122:16-28.
920 Jakab RL, Hamori J (1988) Quantitative morphology and synaptology of cerebellar glomeruli in the rat.
921 Anat Embryol (Berl) 179:81-88.
922 Ji Z, Hawkes R (1994) Topography of Purkinje cell compartments and mossy fiber terminal fields in
923 lobules II and III of the rat cerebellar cortex: spinocerebellar and cuneocerebellar projections.
924 Neuroscience 61:935-954.
925 Jiang J, Azim E, Ekerot CF, Alstermark B (2015) Direct and indirect spino-cerebellar pathways: shared
926 ideas but different functions in motor control. Front Comput Neurosci 9:75.
927 Jorntell H, Ekerot C, Garwicz M, Luo XL (2000) Functional organization of climbing fibre projection to
928 the cerebellar anterior lobe of the rat. J Physiol 522 Pt 2:297-309.
929 Kato S, Kobayashi K, Kobayashi K (2014) Improved transduction efficiency of a lentiviral vector for
930 neuron-specific retrograde gene transfer by optimizing the junction of fusion envelope
931 glycoprotein. J Neurosci Methods 227:151-158.
932 Kim JH, Lee SR, Li LH, Park HJ, Park JH, Lee KY, Kim MK, Shin BA, Choi SY (2011) High cleavage
933 efficiency of a 2A peptide derived from porcine teschovirus-1 in human cell lines, zebrafish and
934 mice. PLoS One 6:e18556.

935 Liang H, Bacskai T, Paxinos G (2015) Termination of vestibulospinal fibers arising from the spinal
936 vestibular nucleus in the mouse spinal cord. Neuroscience 294:206-214.
937 Llewellyn-Smith IJ, Martin CL, Fenwick NM, Dicarlo SE, Lujan HL, Schreihofer AM (2007) VGLUT1 and
938 VGLUT2 innervation in autonomic regions of intact and transected rat spinal cord. J Comp
939 Neurol 503:741-767.
940 Luo Y, Patel RP, Sarpong GA, Sasamura K, Sugihara I (2018) Single axonal morphology and
941 termination to cerebellar aldolase C stripes characterize distinct spinocerebellar projection
942 systems originating from the thoracic spinal cord in the mouse. J Comp Neurol 526:681-706.
943 Madisen L, Zwingman TA, Sunkin SM, Oh SW, Zariwala HA, Gu H, Ng LL, Palmiter RD, Hawrylycz MJ,
944 Jones AR, Lein ES, Zeng H (2010) A robust and high-throughput Cre reporting and
945 characterization system for the whole mouse brain. Nat Neurosci 13:133-140.
946 Madisen L et al. (2015) Transgenic mice for intersectional targeting of neural sensors and effectors with
947 high specificity and performance. Neuron 85:942-958.
948 Malet M, Vieytes CA, Lundgren KH, Seal RP, Tomasella E, Seroogy KB, Hokfelt T, Gebhart GF,
949 Brumovsky PR (2013) Transcript expression of vesicular glutamate transporters in lumbar
950 dorsal root ganglia and the spinal cord of mice - Effects of peripheral axotomy or hindpaw
951 inflammation. Neuroscience 248:95-111.
952 Manni E, Petrosini L (2004) A century of cerebellar somatotopy: a debated representation. Nat Rev
953 Neurosci 5:241-249.
954 Marr D (1969) A theory of cerebellar cortex. J Physiol 202:437-470.
955 Matsushita M, Ikeda M (1970) Spinal projections to the cerebellar nuclei in the cat. Exp Brain Res
956 10:501-511.
957 Matsushita M, Hosoya Y (1979) Cells of origin of the spinocerebellar tract in the rat, studied with the
958 method of retrograde transport of horseradish peroxidase. Brain Res 173:185-200.
959 Matsushita M, Gao X (1997) Projections from the thoracic cord to the cerebellar nuclei in the rat,
960 studied by anterograde axonal tracing. J Comp Neurol 386:409-421.

961 Matsushita M, Hosoya Y, Ikeda M (1979) Anatomical organization of the spinocerebellar system in the
962 cat, as studied by retrograde transport of horseradish peroxidase. J Comp Neurol 184:81-106.
963 Matsushita M, Yaginuma H, Tanami T (1992) Somatotopic termination of the spino-olivary fibers in the
964 cat, studied with the wheat germ agglutinin-horseradish peroxidase technique. Exp Brain Res
965 89:397-407.
966 Miura H, Quadros RM, Gurumurthy CB, Ohtsuka M (2018) Easi-CRISPR for creating knock-in and
967 conditional knockout mouse models using long ssDNA donors. Nat Protoc 13:195-215.
968 Mogensen H, Bengtsson F, Jorntell H (2017) No Medium-Term Spinocerebellar Input Plasticity in Deep
969 Cerebellar Nuclear Neurons In Vivo? Cerebellum 16:638-647.
970 Nanes BA (2015) Slide Set: Reproducible image analysis and batch processing with ImageJ.
971 Biotechniques 59:269-278.
972 Odeh F, Ackerley R, Bjaalie JG, Apps R (2005) Pontine maps linking somatosensory and cerebellar
973 cortices are in register with climbing fiber somatotopy. J Neurosci 25:5680-5690.
974 Oldenbeuving AW, Eisenman LM, De Zeeuw CI, Ruigrok TJ (1999) Inferior olivary-induced expression
975 of Fos-like immunoreactivity in the cerebellar nuclei of wild-type and Lurcher mice. Eur J
976 Neurosci 11:3809-3822.
977 Oscarsson O (1965) Functional Organization of the Spino- and Cuneocerebellar Tracts. Physiol Rev
978 45:495-522.
979 Oscarsson O, Sjolund B (1977a) The ventral spino-olivocerebellar system in the cat. I. Identification of
980 five paths and their termination in the cerebellar anterior lobe. Exp Brain Res 28:469-486.
981 Oscarsson O, Sjolund B (1977b) The ventral spine-olivocerebellar system in the cat. II. Termination
982 zones in the cerebellar posterior lobe. Exp Brain Res 28:487-503.
983 Park YG et al. (2018) Protection of tissue physicochemical properties using polyfunctional crosslinkers.
984 Nat Biotechnol.
985 Paxinos G, Franklin KBJ (2007) The Mouse Brain in Stereotaxic Coordinates, Third Edition. San Diego:
986 Academic Press.

Pijpers A, Ruigrok TJ (2006) Organization of pontocerebellar projections to identified climbing fiber zones in the rat. J Comp Neurol 496:513-528.

Pijpers A, Apps R, Pardoe J, Voogd J, Ruigrok TJ (2006) Precise spatial relationships between mossy fibers and climbing fibers in rat cerebellar cortical zones. J Neurosci 26:12067-12080.

Pivetta C, Esposito MS, Sigrist M, Arber S (2014) Motor-circuit communication matrix from spinal cord to brainstem neurons revealed by developmental origin. Cell 156:537-548.

Popova LB, Ragnarson B, Orlovsky GN, Grant G (1995) Responses of neurons in the central cervical nucleus of the rat to proprioceptive and vestibular inputs. Archives italiennes de biologie 133:31-45.

Quadros RM et al. (2017) Easi-CRISPR: a robust method for one-step generation of mice carrying conditional and insertion alleles using long ssDNA donors and CRISPR ribonucleoproteins. Genome Biol 18:92.

Quinones HI, Savage TK, Battiste J, Johnson JE (2010) Neurogenin 1 (Neurog1) expression in the ventral neural tube is mediated by a distinct enhancer and preferentially marks ventral interneuron lineages. Dev Biol.

Reeber SL, Gebre SA, Sillitoe RV (2011) Fluorescence mapping of afferent topography in three dimensions. Brain Struct Funct 216:159-169.

Rodrigues DM, Li AY, Nair DG, Blennerhassett MG (2011) Glial cell line-derived neurotrophic factor is a key neurotrophin in the postnatal enteric nervous system. Neurogastroenterol Motil 23:e44-56.

Rose MF, Ahmad KA, Thaller C, Zoghbi HY (2009) Excitatory neurons of the proprioceptive, interoceptive, and arousal hindbrain networks share a developmental requirement for Math1. Proc Natl Acad Sci U S A 106:22462-22467.

Sakai N, Insolera R, Sillitoe RV, Shi SH, Kaprielian Z (2012) Axon sorting within the spinal cord marginal zone via Robo-mediated inhibition of N-cadherin controls spinocerebellar tract formation. J Neurosci 32:15377-15387.

1012 Santarcangelo E, Pompeiano O, Stampacchia G (1981) Effects of kainic acid lesions of lateral reticular
1013 nucleus on posture and reflex movements. Archives italiennes de biologie 119:324-340.
1014 Schindelin J, Arganda-Carreras I, Frise E, Kaynig V, Longair M, Pietzsch T, Preibisch S, Rueden C,
1015 Saalfeld S, Schmid B, Tinevez JY, White DJ, Hartenstein V, Eliceiri K, Tomancak P, Cardona A
1016 (2012) Fiji: an open-source platform for biological-image analysis. Nat Methods 9:676-682.
1017 Sengul G, Fu Y, Yu Y, Paxinos G (2015) Spinal cord projections to the cerebellum in the mouse. Brain
1018 Struct Funct 220:2997-3009.
1019 Shambes GM, Gibson JM, Welker W (1978) Fractured somatotopy in granule cell tactile areas of rat
1020 cerebellar hemispheres revealed by micromapping. Brain Behav Evol 15:94-140.
1021 Sherrington CS (1906) The Integrative Action of the Nervous System. New Haven, CT: Yale University
1022 Press.
1023 Sillitoe RV, Fu YH, Watson C (2012) The mouse nervous system. In, 1st Edition (Watson C, Paxinos G,
1024 Puelles L, eds), pp pp.360-397. Amsterdam ; Boston: Elsevier Academic Press.
1025 Soriano P (1999) Generalized lacZ expression with the ROSA26 Cre reporter strain. Nat Genetics
1026 21:70-71.
1027 Sugihara I, Quy PN (2007) Identification of aldolase C compartments in the mouse cerebellar cortex by
1028 olivocerebellar labeling. J Comp Neurol 500:1076-1092.
1029 Suzuki H, Hase A, Miyata Y, Arahata K, Akazawa C (1998) Prominent expression of glial cell line-
1030 derived neurotrophic factor in human skeletal muscle. J Comp Neurol 402:303-312.
1031 Swenson RS, Castro AJ (1983a) The afferent connections of the inferior olivary complex in rats. An
1032 anterograde study using autoradiographic and axonal degeneration techniques. Neuroscience
1033 8:259-275.
1034 Swenson RS, Castro AJ (1983b) The afferent connections of the inferior olivary complex in rats: a study
1035 using the retrograde transport of horseradish peroxidase. Am J Anat 166:329-341.

1036 Szabo T, Libouban S, Denizot JP (1990) A well defined spinocerebellar system in the weakly electric
1037 teleost fish Gnathonemus petersii. A tracing and immuno-histochemical study. Archives
1038 italiennes de biologie 128:229-247.
1039 Trupp M, Ryden M, Jornvall H, Funakoshi H, Timmusk T, Arenas E, Ibanez CF (1995) Peripheral
1040 expression and biological activities of GDNF, a new neurotrophic factor for avian and
1041 mammalian peripheral neurons. J Cell Biol 130:137-148.
1042 Tuthill JC, Azim E (2018) Proprioception. Curr Biol 28:R194-R203.
1043 Voogd J, Ruigrok TJ (2004) The organization of the corticonuclear and olivocerebellar climbing fiber
1044 projections to the rat cerebellar vermis: the congruence of projection zones and the zebrin
1045 pattern. J Neurocytol 33:5-21.
1046 Voogd J, Pardoe J, Ruigrok TJ, Apps R (2003) The distribution of climbing and mossy fiber collateral
1047 branches from the copula pyramidis and the paramedian lobule: congruence of climbing fiber
1048 cortical zones and the pattern of zebrin banding within the rat cerebellum. J Neurosci 23:4645-
1049 4656.
1050 Watson C, Paxinos G, Kayalioglu G (2009) The Spinal Cord: A Christopher and Dana Reeve
1051 Foundation Text and Atlas. New York: Academic Press.
1052 White JJ, Sillitoe RV (2017) Genetic silencing of olivocerebellar synapses causes dystonia-like
1053 behaviour in mice. Nat Commun 8:14912.
1054 Wiksten B (1987) Further studies on the fiber connections of the central cervical nucleus in the cat. Exp
1055 Brain Res 67:284-290.
1056 Windhorst U (2007) Muscle proprioceptive feedback and spinal networks. Brain Res Bull 73:155-202.
1057 Yang H, Xie X, Deng M, Chen X, Gan L (2010) Generation and characterization of Atoh1-Cre knock-in
1058 mouse line. Genesis 48:407-413.
1059 Yuengert R, Hori K, Kibodeaux EE, McClellan JX, Morales JE, Huang TW, Neul JL, Lai HC (2015)
1060 Origin of a Non-Clarke's Column Division of the Dorsal Spinocerebellar Tract and the Role of
1061 Caudal Proprioceptive Neurons in Motor Function. Cell Rep 13:1258-1271.

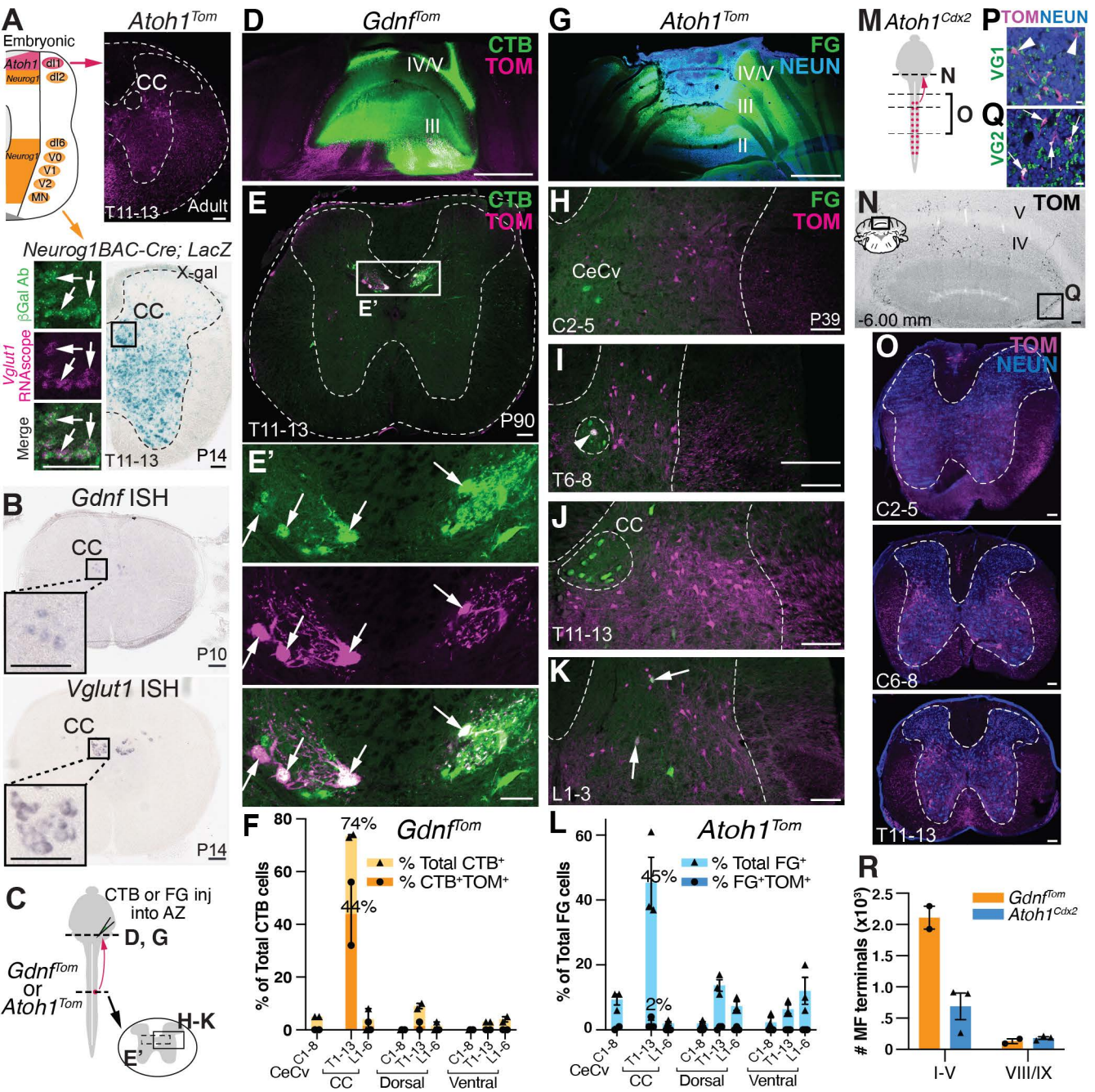

Figure 1. Clarke's column (CC) is the major direct spinocerebellar pathway in mice. (A) Lineage tracing of *Neurog1*-expressing progenitors (*Neurog1BAC-Cre* crossed to *R26*$^{LSL\text{-}LacZ}$) in the neural tube identifies large CC neurons in the thoracic spinal cord (box in X-gal stain). β-Gal expressing cells (green) colocalize with the CC marker, *Vglut1* mRNA (magenta, arrows). *Atoh1*-lineage neurons (*Atoh1*^{Tom}) reside lateral and ventral to CC. (B) CC is marked by expression of *Gdnf* and *Vglut1* mRNA. (C) Diagram of cerebellar injections into the anterior zone (AZ, lobules I-V) with either CTB or fluorogold (FG) into either *Gdnf*^{Tom} or *Atoh1*^{Tom} mice to retrogradely label direct spinocerebellar projections. (D-E') CTB injection into vermis lobules III-V of the cerebellum retrogradely labels CC (E, E', green) in the spinal cord and colocalizes with the genetic label for CC (*Gdnf*^{Tom})(E', CTB^{+}TOM^{+}, arrows). (F) Quantitation of the percentage of total CTB^{+} cells in a given region of the spinal cord (light orange) with the percentage of CTB^{+}TOM^{+} cells superimposed (dark orange). 74 ± 1% (n=2) of all CTB^{+} cells in the spinal cord are in CC T1-13. 44 ± 12% of all CTB^{+} cells are TOM^{+} in CC T1-13. Therefore, 60 ± 16% of CTB^{+} neurons in CC are labeled by *Gdnf*^{Tom}. Spinal cords were divided into cervical (C), thoracic (T), and lumbar (L) areas. The central cervical (CeCv) and CC areas were delineated separately with all other cells categorized based on their C, T, L, S location and whether they were dorsal or ventral to the central canal. (G) FG injected into vermis lobules II-V of *Atoh1*^{Tom} mice. (H-K) Retrograde labeling from the cerebellum with FG (green) labels CC (I, J) in the thoracic spinal cord, CeCv in the cervical spinal cord (H), and a few other neurons in other areas of the spinal cord (K). Only a few neurons are *Atoh1*-lineage (K, FG^{+}TOM^{+}, arrows) with an occasional *Atoh1*-lineage neuron labeling a CC cell (I, FG^{+}TOM^{+}, arrowhead) as previously reported (Yuengert et al., 2015). (L) Quantitation of the percentage of FG^{+} cells in a given region of the spinal cord (light blue) with the percentage of FG^{+}TOM^{+} cells superimposed (dark blue). FG retrogradely labels mostly CC neurons in T1-13 (45 ± 8%, n=3) with 2 ± 1% of total FG^{+} cells being FG^{+}TOM^{+} in CC T1-13. Therefore, only 4% ± 1% of FG^{+} cells in CC T1-13 are labeled with *Atoh1*^{Tom}. (M-N) In mice where caudal *Atoh1*-lineage neurons are labeled (*Atoh1*^{Cdx2}), few mossy fiber (MF) terminals are seen in the cerebellum (N). (O) Spinal cord neurons caudal to C2-5 are labeled with tdTomato (TOM^{+}, magenta) in *Atoh1*^{Cdx2} mice. Few cell bodies in the C2-5 spinal cord area are TOM^{+} compared to C6-8 and T11-13 sections. NEUN antibody staining (blue) delineates the grey matter of the spinal cord. (P-Q) *Atoh1*^{Cdx2} TOM^{+} MF terminals are VGLUT1^{-} (P, arrowheads) and VGLUT2^{+} (Q, arrows). (R) Counts from comparable sections of *Gdnf*^{Tom} and *Atoh1*^{Cdx2} mice indicate that neurons labeled in *Atoh1*^{Cdx2} mice have considerably fewer MF terminals in lobules I-V (*Gdnf*^{Tom} 2110 ± 183 terminals, n=2 vs. *Atoh1*^{Cdx2} 690 ± 265 terminals, n=3), while MF terminals in lobules VIII/IXa are comparable (*Gdnf*^{Tom} 130 ± 37 terminals vs. *Atoh1*^{Cdx2} 137 ± 55 terminals). Abbrev: P, postnatal. Scale bars: 1 mm (D, G), 100 μm (A, B, E, E', H-K, N, O), 10 μm (P,Q).

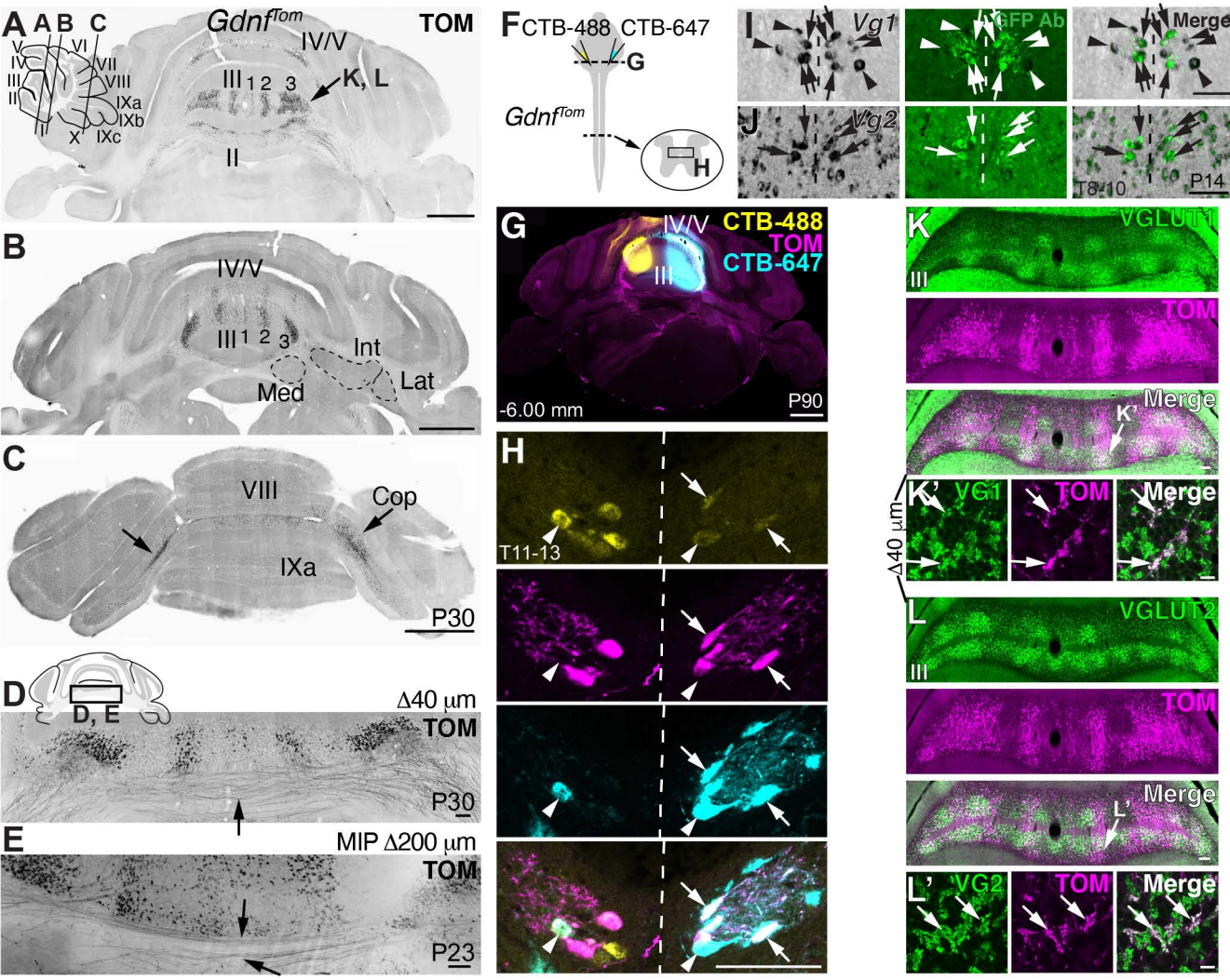

Figure 2. Glutamatergic CC mossy fibers terminate ipsilaterally and contralaterally in the cerebellar vermis. (A-C) Coronal sections from *Gdnf*^{Tom} mice reveal CC mossy fiber (MF) terminals (TOM^{+}) in lobules II-V, VIII, IXa, and the copula (C, Cop, arrows). Parasagittal stripes (1, 2, 3) in lobule III are apparent. (D-E) Some CC axons (TOM^{+}) cross the midline (D, arrow, cryosection, and E, arrows, cleared sample, 200 μm maximum intensity projection (MIP)). (F) Diagram of dual CTB-488 and CTB-647 injections in *Gdnf*^{Tom} mice. (G) Coronal section showing the injection site of CTB-488 and CTB-647. (H) CC neurons are co-labeled with the fluorescent CTB injected on the ipsilateral side as well as the fluorescent CTB injected on the contralateral side (arrows and arrowheads, CTB-488^{+}CTB-647^{+}). Some cells also colocalize with the *Gdnf*^{Tom} genetic label for CC (arrowheads, TOM^{+}CTB-488^{+}CTB-647^{+}). (I-J) CC cells in the spinal cord (GFP^{+} antibody) express both *Vglut1* (*Vg1*) and *Vglut2* (*Vg2*) mRNA (arrows, *Gdnf*^{EYFP} mice, GFP antibody to amplify signal). *Gdnf*^{EYFP} mice injected with tamoxifen at P7 reveal that only a subset of CC is labeled (I, *Vg1*$^{+}$-only cells, arrowheads). (K-L') CC MF terminals (TOM^{+}) overlap with VGLUT1 (K-K') and VGLUT2 (L-L') stripes in lobule III. K and L panels are neighboring 40 μm sections taken from lobule III indicated in (A, arrow). Abbrev: Med, Medial; Int, Interpositus; Lat, Lateral. Scale bars: 1 mm (A, B, C, G), 100 μm (D, E, H, I, J, K, L), 10 μm (K', L').

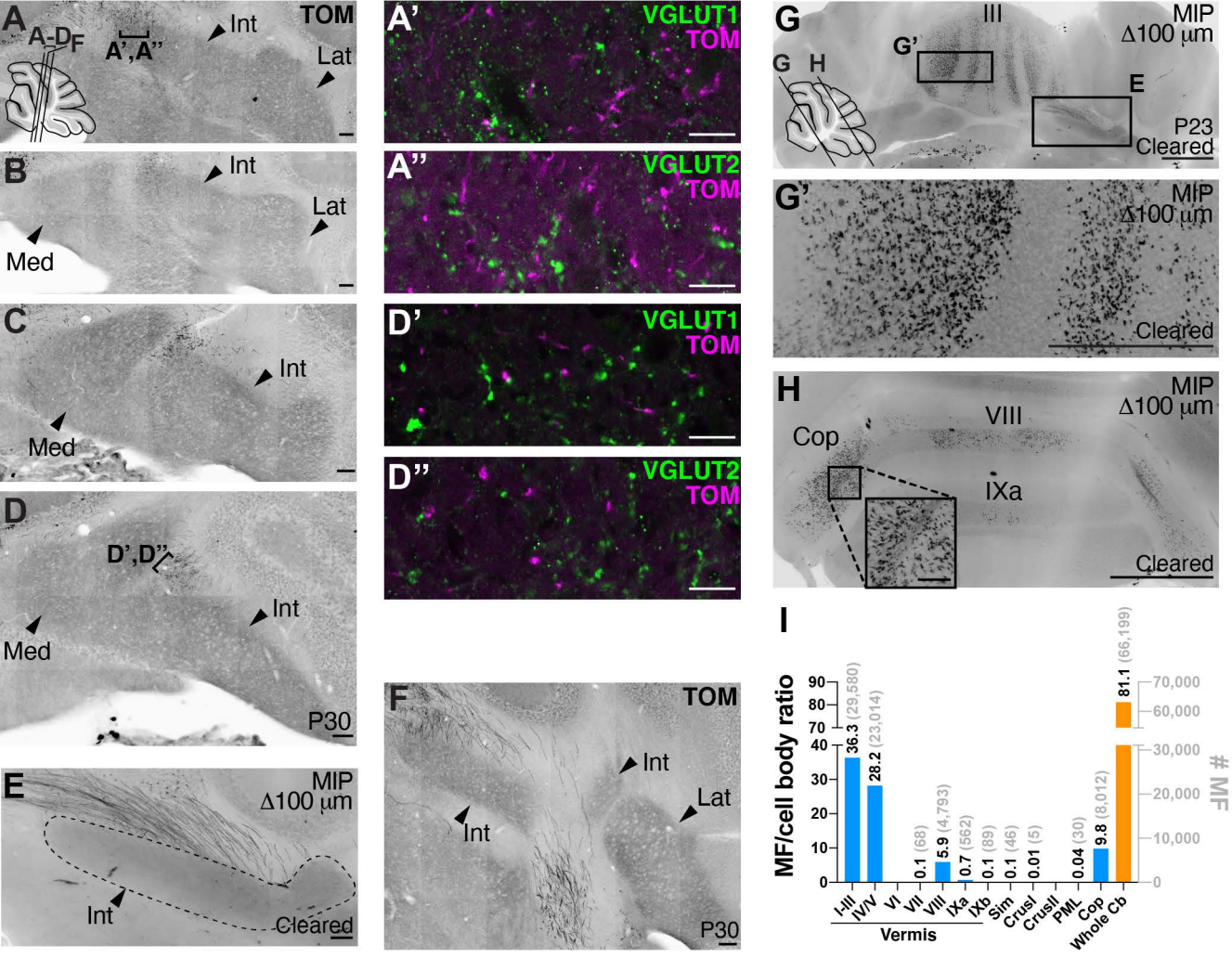

Figure 3. CC neurons evade the cerebellar nuclei (CN) and arborize extensively in the cerebellar cortex. (A-D) Almost no CC *Gdnf*^{Tom} axons enter or are near the CN (arrowheads, Med, Int, Lat)(A, B, C, and D are successive sections 160 μm apart). Areas of TOM^{+} signal near CN do not colocalize with presynaptic markers VGLUT1 (A', D') or VGLUT2 (A", D") indicating these are axons of passage and not presynaptic terminals. (E) CC axons (TOM^{+}) avoid the CN in another *Gdnf*^{Tom} mouse whose cerebellum was cleared (100 μm MIP). (F) CC axons (TOM^{+}) avoid the CN (40 μm cryosection) in another example *Gdnf*^{Tom} mouse. Images are from two female (A-E) and one male (F) mice (n=3). (G-H) Example images of 100 μm MIP from a *Gdnf*^{Tom} cleared cerebellum. CC MF terminals (TOM^{+}) are seen in II-V, VIII, IXa, and Cop. (I) The total number of MF terminals (grey) were counted from each region of the cerebellum in the cleared sample (n=1, see Material and Methods) and divided by the total number of *Gdnf*^{Tom} CC cell bodies (816 cells) in the spinal cord of the cleared sample (black, MF/cell body ratio). Overall the whole cerebellum (Cb) has an estimated 81.1 MF terminals per CC cell body in the spinal cord (orange bar). Most MF terminals from *Gdnf*^{Tom} CC cells terminate in I-III, IV/V, VIII/IXa, and Cop (blue bars). Abbrev: Med, Medial; Int, Interpositus; Lat, Lateral. Scale bars: 1 mm (G, G', H), 100 μm (H inset, A-F), 10 μm (A'-A", D'-D").

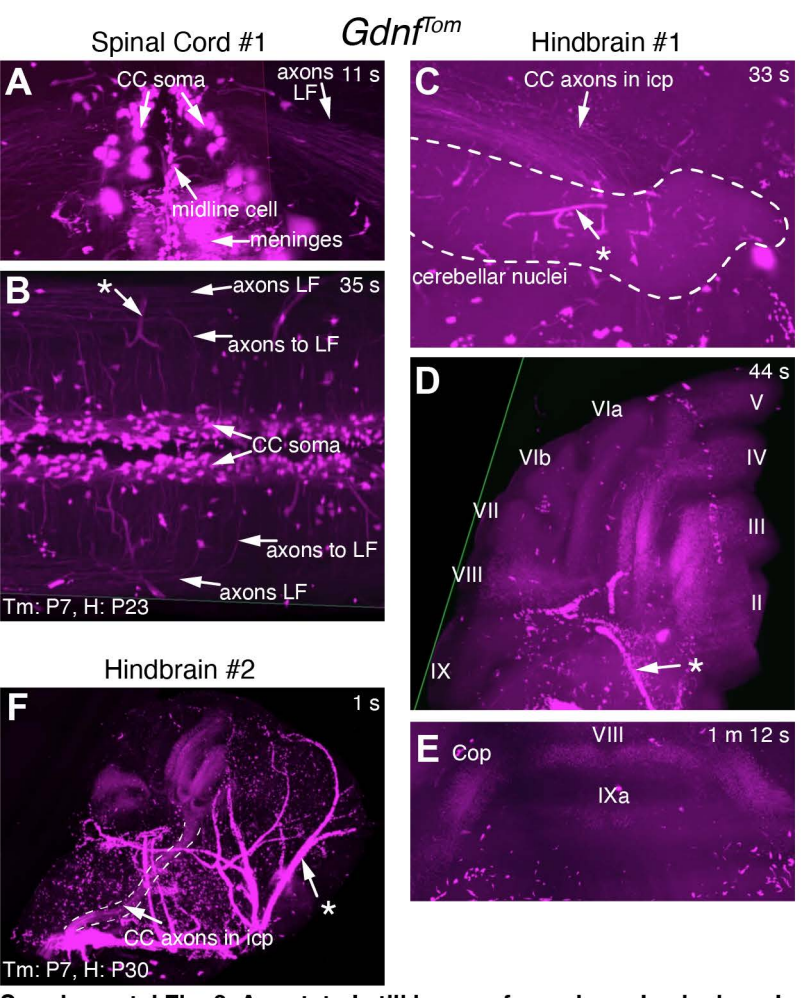

Supplemental Fig. 3. Annotated still images from cleared spinal cords and hindbrains. (A-B) Screenshots of spinal cord sample #1. CC cell bodies (soma) cluster around the midline mainly in the thoracic region of the spinal cord (TOM$^+$, magenta). Axons are seen extending toward the LF and extending rostrally. Unidentified midline cells and smooth muscle cells lining blood vessels (*) are labeled with the *Gdnf^{Tom}* mouse line. The meninges also fluoresces. (C-E) Screenshots of hindbrain sample #1. CC axons avoid the cerebellar nuclei and terminate in I-V, VIII, IXa, and Cop. (F) Screenshot of hindbrain sample #2. CC axons are seen traveling rostrally from the spinal cord through the icp. Smooth muscle cells lining blood vessels (*) are prominently labeled in this sample. Time stamp from which the screenshot was taken is in the upper right corner. Abbrev: LF, lateral funiculus; icp, inferior cerebellar peduncle.

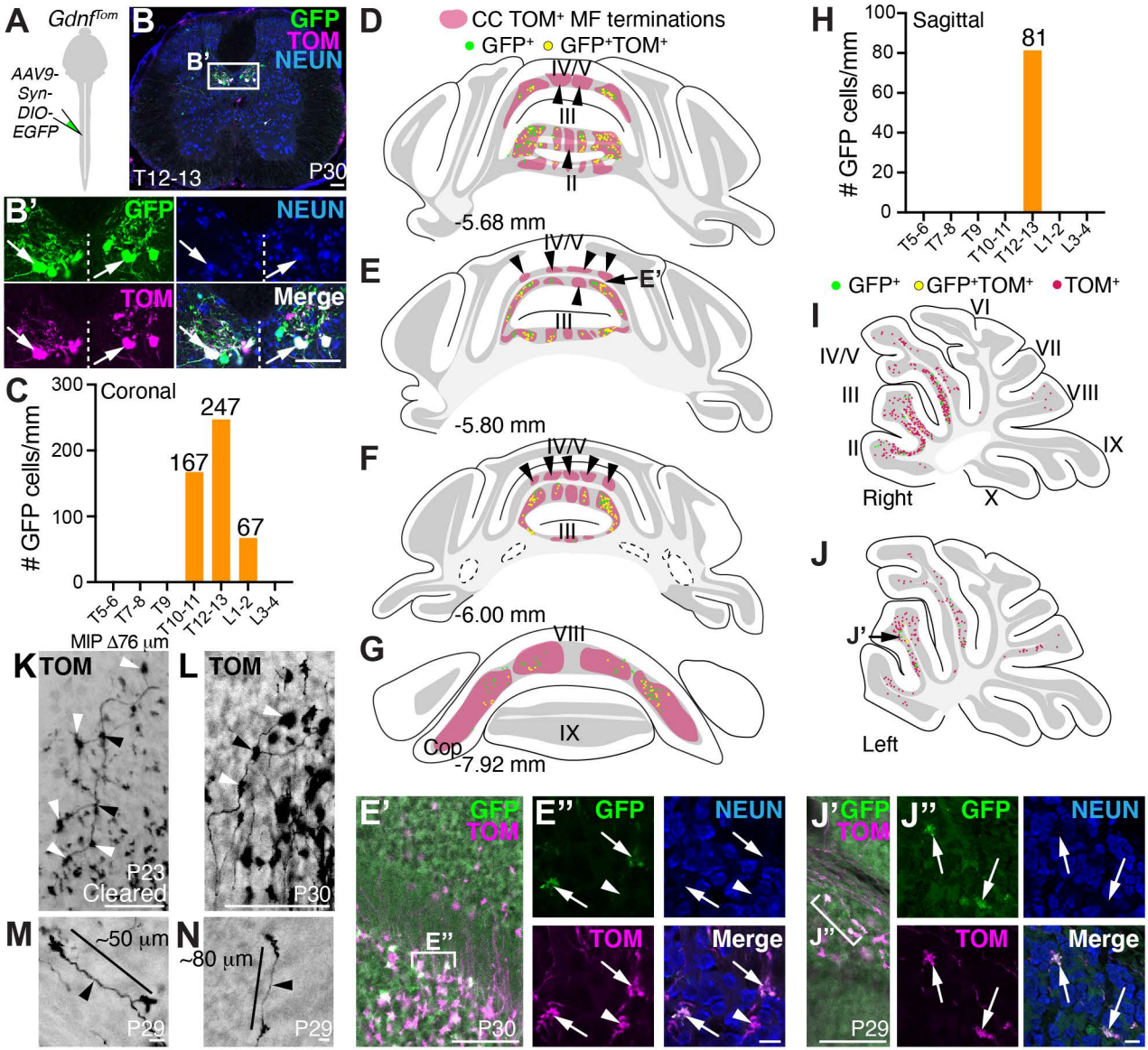

Figure 4. Thoracolumbar CC MFs send diverse projections to multiple lobules. (A-B') Spinal cord injections of AAV9-Syn-DIO-EGFP at lower thoracic levels into *Gdnf*^{Tom} mice labels CC neurons on both sides of the spinal cord (B', arrows). (C) GFP$^+$ cells for one experiment are expressed mainly in the T10-L2 region of the spinal cord. (D-G) Schematics of coronal cerebellar sections of the spinal cord injected from C indicating the location of all CC MF terminations (TOM$^+$, red areas). The subset of CC MF terminations that are from the lower thoracic-lumbar region (GFP$^+$, green, and GFP$^+$TOM$^+$, yellow) are spread over multiple lobules (II-V, VIII). Certain CC MF termination regions do not have thoracolumbar CC neuronal projections (red areas, arrowheads with an absence of any GFP$^+$ terminations). (E'-E'') Example of CC MF terminations (TOM$^+$, arrows and arrowhead), some of which are from the thoracolumbar spinal cord (GFP$^+$TOM$^+$, arrows). (H) GFP$^+$ cells in a second injection are expressed mainly in the T12-13 region of the spinal cord. (I-J) Sagittal cerebellar views of the AAV9-Syn-DIO-EGFP-injected *Gdnf*^{Tom} mouse from H. Thoracolumbar CC MF terminals (GFP$^+$, green, and GFP$^+$TOM$^+$, yellow) are spread out over lobules II-V. All CC MF terminals are TOM$^+$ (I-J, red dots). (J'-J'') Thoracolumbar CC MF terminations (GFP$^+$TOM$^+$, arrows) are seen in lobule III. (K-N) Examples of individual MF axons and terminals from three mice: a cleared female mouse sample (K, 76 μm maximum intensity projection (MIP)), one female mouse (L, 40 μm cryosection), and one male mouse (M, N, 40 μm cryosection). Axons appear to have branching points (black arrowheads) and regularly spaced MF terminals (white arrowheads)(K-L). MF terminals from an individual axon are spaced 50-80 μm apart (M-N). Scale bars: 100 μm (B, B', E', J', K, L); 10 μm (E'', J'', M, N).

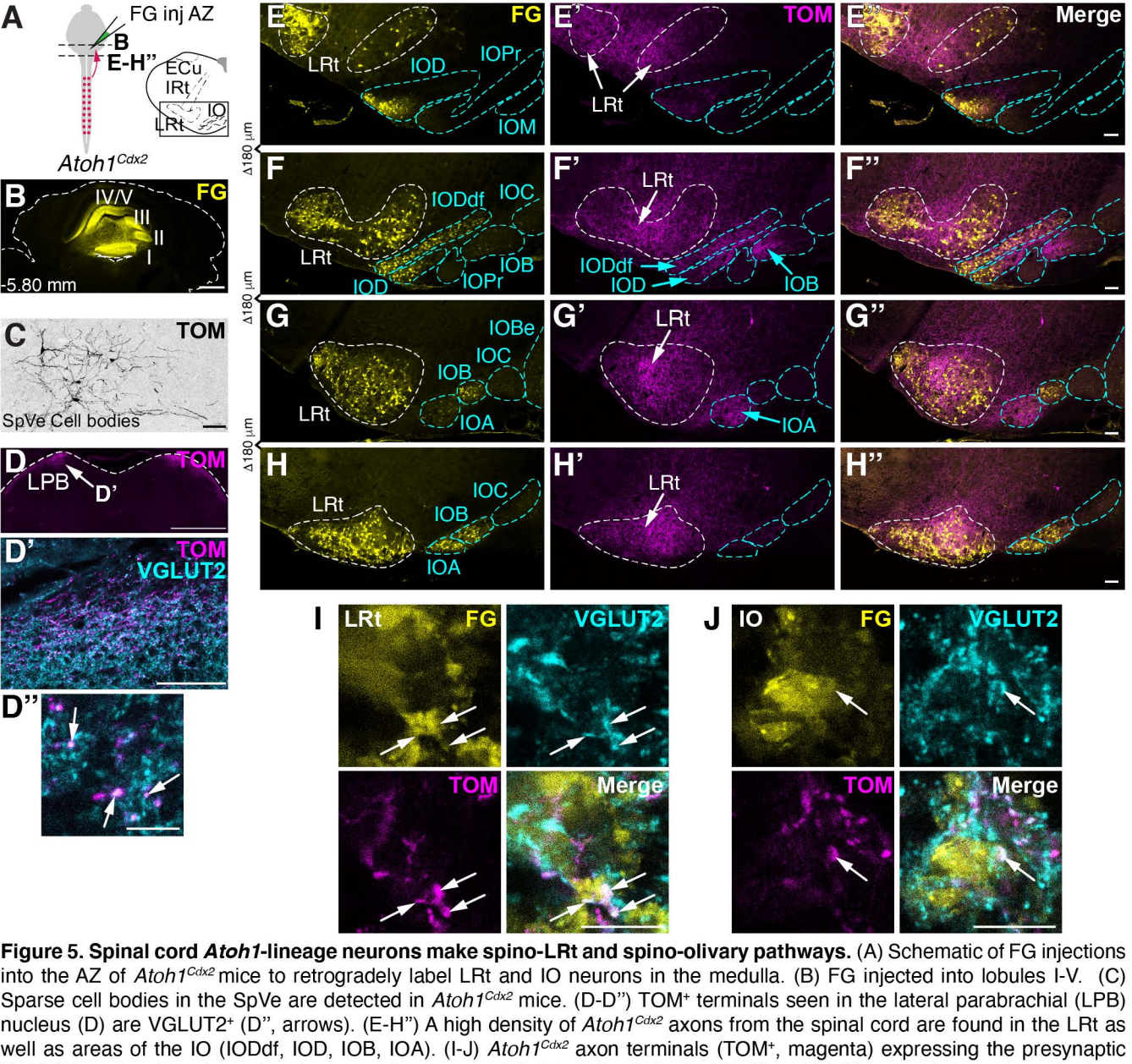

Figure 5. Spinal cord *Atoh1*-lineage neurons make spino-LRt and spino-olivary pathways. (A) Schematic of FG injections into the AZ of *Atoh1*^{Cdx2} mice to retrogradely label LRt and IO neurons in the medulla. (B) FG injected into lobules I-V. (C) Sparse cell bodies in the SpVe are detected in *Atoh1*^{Cdx2} mice. (D-D”) TOM^{+} terminals seen in the lateral parabrachial (LPB) nucleus (D) are VGLUT2^{+} (D”, arrows). (E-H”) A high density of *Atoh1*^{Cdx2} axons from the spinal cord are found in the LRt as well as areas of the IO (IODdf, IOD, IOB, IOA). (I-J) *Atoh1*^{Cdx2} axon terminals (TOM^{+}, magenta) expressing the presynaptic VGLUT2 marker (cyan) are closely apposed to retrogradely labeled cells in the LRt (I) and IO (J)(arrows). Axonal terminations in the LRt and IO were verified in n=4 mice. Representative sections shown in E-H”. Abbrev: ECu, external cuneate nucleus; IO, inferior olive; IOA, inferior olive subnucleus A of medial nucleus; IOB, inferior olive subnucleus B of medial nucleus; IOBe, inferior olive beta subnucleus; IOC, inferior olive subnucleus C of medial nucleus; IOD, inferior olive dorsal nucleus; IODdf, dorsal fold of the IOD; IOM, inferior olive medial nucleus; IOPr, inferior olive principal nucleus; IRt, intermediate reticular nucleus; LRt, lateral reticular nucleus; SpVe, spinal vestibular nucleus. Scale bars: 1 mm (B, D), 100 μm (C, D’, E-H”), 10 μm (D”, I, J).

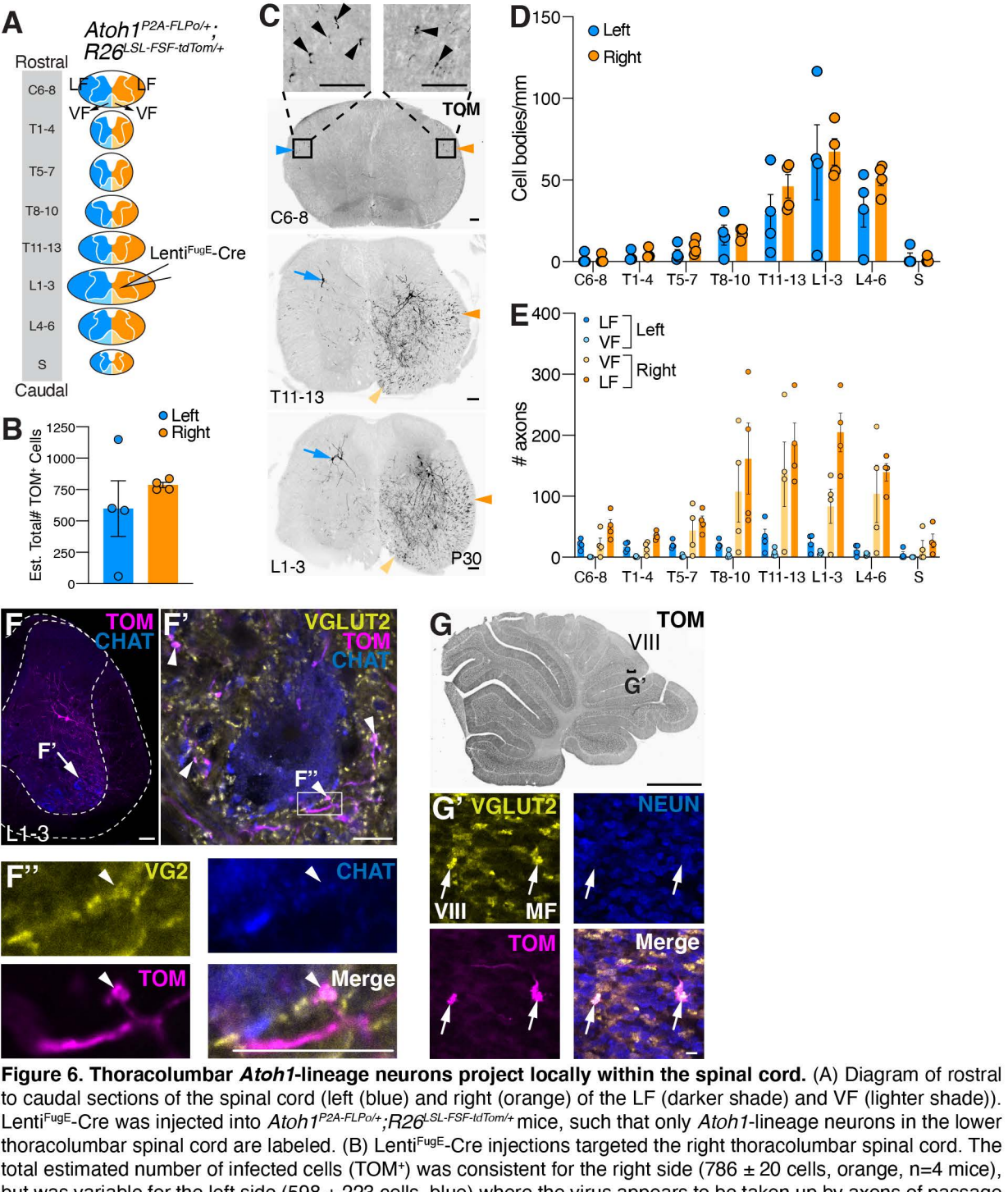

Figure 6. Thoracolumbar *Atoh1*-lineage neurons project locally within the spinal cord. (A) Diagram of rostral to caudal sections of the spinal cord (left (blue) and right (orange) of the LF (darker shade) and VF (lighter shade)). Lenti^{FugE}-Cre was injected into *Atoh1*$^{P2A\text{-}FLPo/+}$;*R26*$^{LSL\text{-}FSF\text{-}tdTom/+}$ mice, such that only *Atoh1*-lineage neurons in the lower thoracolumbar spinal cord are labeled. (B) Lenti^{FugE}-Cre injections targeted the right thoracolumbar spinal cord. The total estimated number of infected cells (TOM$^+$) was consistent for the right side (786 ± 20 cells, orange, n=4 mice), but was variable for the left side (598 ± 223 cells, blue) where the virus appears to be taken up by axons of passage that project to the contralateral side (see C). (C) Representative sections of the spinal cord from a Lenti^{FugE}-Cre-injected *Atoh1*$^{P2A\text{-}FLPo/+}$;*R26*$^{LSL\text{-}FSF\text{-}tdTom/+}$ mouse. Cell bodies on the right side of the spinal cord and axons in the right LF (dark orange arrowhead) are labeled. Axons in the right VF (light orange arrowhead) appear to be axons from cell bodies that are located on the contralateral side of the spinal cord (blue arrows). Some axons in the left LF (blue arrowhead) are also seen. (D) L1-3 is the site of peak infection (number of TOM$^+$ cell bodies labeled per length of spinal cord (mm)) and the number of cell bodies labeled tapers off both rostrally and caudally further away from the injection site. (E) Very few axons on the right side (orange (LF) and light orange (VF)) are detected in rostral sections (C6-8) compared to the site of injection L1-3. (F-F'') Some of the sparsely labeled thoracolumbar *Atoh1*-lineage neurons have presynaptic terminals near (arrowheads, TOM$^+$VGLUT2$^+$) or closely apposed (F'', arrowhead, TOM$^+$VGLUT2$^+$) to motor neurons (CHAT$^+$)(detected in n=4 samples, representative image shown). (G-G') Very few MF terminals are detected in the cerebellum. Of the MF terminals that are detected, they are VGLUT2$^+$ (G'). See Materials and Methods for details of quantitation for B, D, E. Abbrev: LF, lateral funiculus; VF, ventral funiculus. Scale bars: 1 μm (G), 100 μm (C, F), 10 μm (F', G', F'').

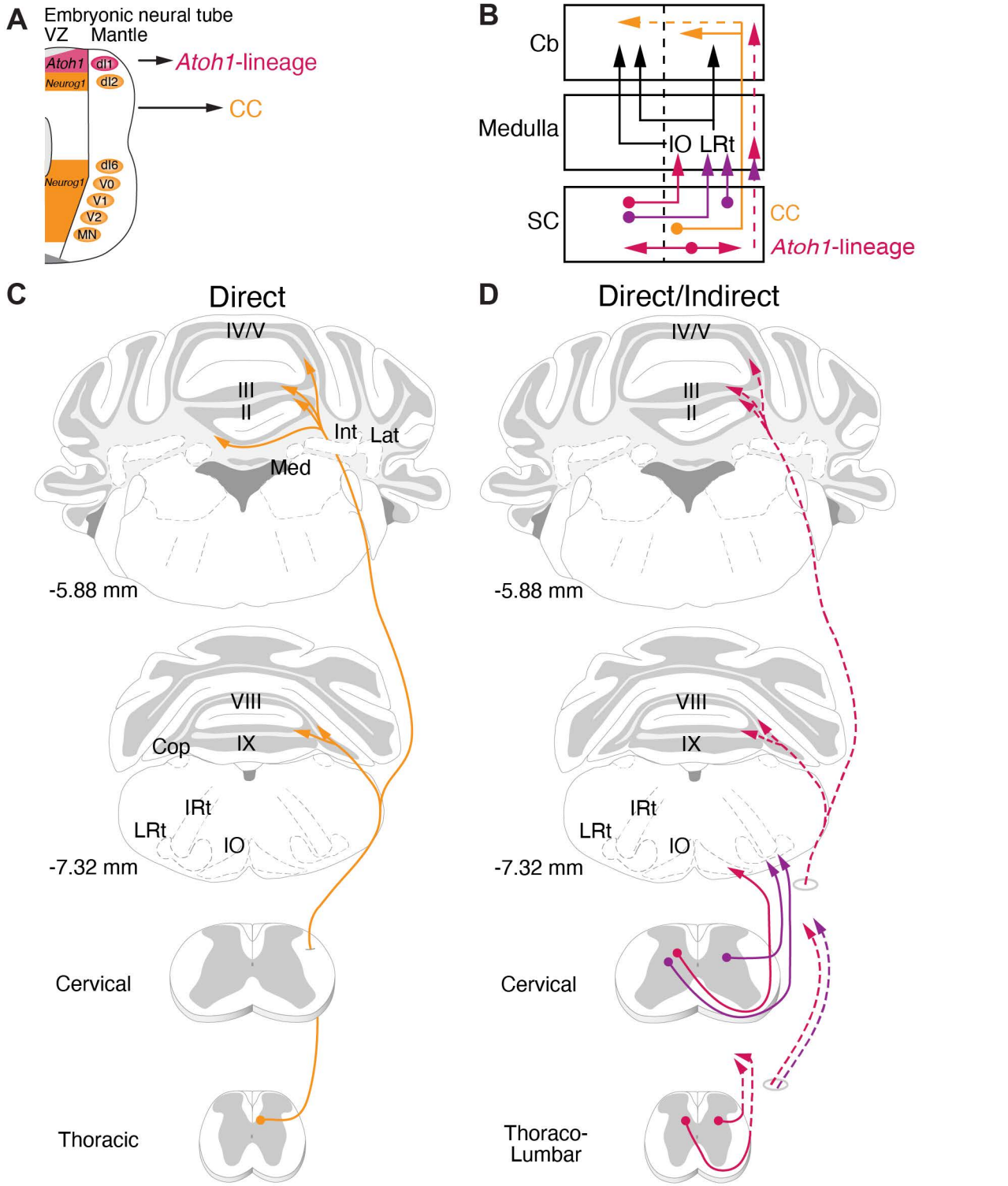

Figure 7. Direct and indirect pathways to the cerebellum. (A) *Neurog1*-lineage neurons of the developing neural tube generate CC neurons that project directly from the spinal cord to the cerebellum while *Atoh1*-lineage neurons form both direct and indirect pathways to the cerebellum. (B) Schematic of major anatomical findings. CC neurons (orange) project ipsilaterally mainly from the thoracic spinal cord directly to the cerebellum. Some CC axons cross the midline (dotted orange). *Atoh1*-lineage neurons project mainly to the IO and LRt in the medulla (red and purple). Thoracolumbar *Atoh1*-lineage neurons project mostly within the spinal cord (red, horizontal arrows), although some project to more rostral regions within the medulla and cerebellum (dotted red with purple and red arrowheads). (C-D) Illustrations of direct and indirect spinocerebellar pathways. CC neurons project rostrally in the ipsilateral funiculus where they branch extensively, avoiding the cerebellar nuclei (Med, Int, Lat) to terminate in vermis I-V, VIII, IXa, and Cop (C). Some CC axons cross the midline within the cerebellum. *Atoh1*-lineage neurons in the spinal cord project both ipsilaterally and contralaterally to target mainly the LRt and IO in the hindbrain (D). *Atoh1*-lineage neurons in the thoracolumbar area project mostly locally within the spinal cord. A few of the axons from thoracolumbar *Atoh1*-lineage neurons may project to the medulla (dotted red and purple). Some spinal cord *Atoh1*-lineage neurons reach the AZ (lobules I-V) and PZ (lobules VIII/IXa) of the cerebellar cortex (dotted red). Abbrev: IRt, intermediate reticular nucleus; LRt, lateral reticular nucleus; IO, inferior olive; AZ, anterior zone; PZ, posterior zone.